RAF1-MEK/ERK pathway-dependent ARL4C expression promotes ameloblastoma cell proliferation and osteoclast formation

Fujii, Shinsuke
Laboratory of Oral Pathology, Division of Maxillofacial Diagnostic and Surgical Sciences, Faculty of Dental Science Kyushu University

Ishibashi, Takuma
Laboratory of Oral Pathology, Division of Maxillofacial Diagnostic and Surgical Sciences, Faculty of Dental Science Kyushu University

Kokura, Megumi
Laboratory of Oral Pathology, Division of Maxillofacial Diagnostic and Surgical Sciences, Faculty of Dental Science Kyushu University

Fujimoto, Tatsufumi
Laboratory of Oral Pathology, Division of Maxillofacial Diagnostic and Surgical Sciences, Faculty of Dental Science Kyushu University

他

出版情報：The Journal of Pathology. 256 (1), pp.119-133, 2021-12-13. Wiley
バージョン：

ARL4C expression, due to RAF1-MEK/ERK pathway, promotes ameloblastoma cell proliferation and osteoclast formation

A short running title: ARL4C expression in ameloblastoma

Shinsuke Fujii[1*], Takuma Ishibashi[1 †], Megumi Kokura[1 †], Tatsufumi Fujimoto[1], Shinji Matsumoto[2,3], Satsuki Shidara[1,11], Kari J Kurppa[4], Judith Pape[5], Javier Caton[6], Peter R Morgan[7], Kristiina Heikinheimo[8], Akira Kikuchi[2], Eijiro Jimi[9,10] and Tamotsu Kiyoshima[1]

[1]Laboratory of Oral Pathology, Division of Maxillofacial Diagnostic and Surgical Sciences, Faculty of Dental Science, Kyushu University, 3-1-1 Maidashi, Higashi-ku, Fukuoka 812-8582, Japan

[2]Department of Molecular Biology and Biochemistry, Graduate School of Medicine, Osaka University, 2-2 Yamadaoka, Suita 565-0871, Japan

[3]Integrated Frontier Research for Medical Science Division, Institute for Open and Transdisciplinary Research Initiatives (OTRI), Osaka University, Suita 565-0871, Japan

[4]Institute of Biomedicine and MediCity Research Laboratories, University of Turku, and Turku Bioscience Centre, University of Turku and Åbo Akademi University, Turku, FI-20520, Finland

[5]Division of Surgery and Interventional Science, Department of Targeted Intervention, Centre for 3D Models of Health and Disease, University College London, Gower Street, London, WC1E 6BT, UK

[6]Department of Anatomy and Embryology, Faculty of Medicine, University Complutense Madrid, 28040 Madrid, Spain

[7]Head & Neck Pathology, King's College London, Guy's Hospital, London, SE1 9RT, UK

[8]Department of Oral and Maxillofacial Surgery, Institute of Dentistry, University of Turku and Turku University Hospital, FI-20520, Finland

[9]Oral Health/Brain Health/Total Health Research Center, Faculty of Dental Science, Kyushu University, 3-1-1 Maidashi, Higashi-ku, Fukuoka 812-8582, Japan

[10]Laboratory of Molecular and Cellular Biochemistry, Faculty of Dental Science, Kyushu University, 3-1-1 Maidashi, Higashi-ku, Fukuoka 812-8582, Japan

[11]Present address: Department of Orthodontics, Tokyo Dental College, 1-2-2 Masago, Mihamaku, Chiba 261-8502, Japan

[†]These authors contributed equally to this work as second authors.

[*]Corresponding author. Laboratory of Oral Pathology, Division of Maxillofacial Diagnostic and Surgical Sciences, Faculty of Dental Science, Kyushu University

3-1-1 Maidashi, Higashi-ku, Fukuoka 812-8582, Japan

Phone: +81-92-642-6328; Fax: +81-92-642-6329

E-mail: sfujii@dent.kyushu-u.ac.jp

Conflict of interest statements: No conflicts of interests were declared.

This manuscript has not been published and is not under consideration for publication elsewhere.

A word count: 3,972/4,000

ABSTRACT

Ameloblastoma is an odontogenic neoplasm characterized by slow intraosseous growth with progressive jaw resorption. Recent reports have revealed that ameloblastoma harbors an oncogenic *BRAF* V600E mutation with mitogen-activated protein kinase (MAPK) pathway activation and described cases of ameloblastoma harboring a *BRAF* V600E mutation in which patients were successfully treated with a BRAF inhibitor. Therefore, the MAPK pathway may be involved in the development of ameloblastoma; however, the precise mechanism by which it induces ameloblastoma is unclear. The expression of ADP-ribosylation factor (ARF)-like 4c (ARL4C), induced by a combination of the EGF-MAPK pathway and Wnt/β-catenin signaling, has been shown to induce epithelial morphogenesis. It was also reported that the overexpression of ARL4C, due to alterations in the EGF/RAS-MAPK pathway and Wnt/β-catenin signaling, promotes tumorigenesis. However, the roles of ARL4C in ameloblastoma are unknown. We investigated the involvement of ARL4C in the development of ameloblastoma. In immunohistochemical analyses of tissue specimens obtained from 38 ameloblastoma patients, ARL4C was hardly detected in non-tumour regions but tumours frequently showed strong expression of ARL4C, along with the expression of both BRAF V600E and RAF1 (also known as C-RAF). Loss-of-function experiments using inhibitors or siRNAs revealed that ARL4C elevation depended on the RAF1-MEK/ERK pathway in ameloblastoma cells. It was also shown that the RAF1-ARL4C and BRAF V600E-MEK/ERK pathways promoted cell proliferation independently. ARL4C-depleted tumour cells (generated by knockdown or knockout) exhibited decreased proliferation and migration capabilities. Finally, when ameloblastoma cells were co-cultured with mouse bone marrow cells and primary osteoblasts, ameloblastoma cells induced osteoclast formation. ARL4C elevation in

ameloblastoma further promoted its formation capabilities through the increased RANKL expression of mouse bone marrow cells and/or primary osteoblasts. These results suggest that the RAF1-MEK/ERK-ARL4C axis, which may function in cooperation with the BRAF V600E-MEK/ERK pathway, promotes ameloblastoma development.

Key words: Ameloblastoma, ARL4C, BRAF V600E, RAF1, Proliferation, Osteoclast formation

INTRODUCTION

Ameloblastoma, which originates from the dental lamina, is classified as a benign epithelial odontogenic tumour, showing slow intraosseous growth with progressive bone resorption of the jaw [1]. Ameloblastoma is the most common odontogenic tumour, excluding odontomas, tending to recur locally if not adequately removed. Clinically, with increased size, complications include loosening of teeth, malocclusion, paraesthesia, pain, limited mouth opening, difficult mastication and airway obstruction [1]. The main treatment is wide surgical resection with an area of bone beyond radiographic margins; this necessarily results in facial deformity [2]. Ameloblastomas are classified as ameloblastoma (also called conventional ameloblastoma or solid/multicystic ameloblastoma), unicystic ameloblastoma, extraosseous/peripheral ameloblastoma and metastasizing ameloblastoma. Unicystic ameloblastoma is further classified into luminal, intraluminal and mural subtypes [3]. The common histopathological patterns of ameloblastoma are follicular and plexiform [1]. The definitive underlying the pathogenic mechanisms of ameloblastoma, including an increase in ameloblastoma cells and enhanced bone resorption capabilities through osteoclast formation, remain unclear. Therefore, a novel tumour therapy based on the molecular mechanisms underlying ameloblastoma development is awaited.

In the age of precision cancer medicine, tumour specimens are processed for next-generation sequencing with gene panel tests to detect gene mutations/variants for optimizing therapeutic intervention [4]. As ameloblastomas are rare, with an incidence of 0.5 cases per million population [1,5], information concerning the molecular mechanisms involved in the aetiology of ameloblastoma is limited. It is thus necessary to investigate the roles of individual signal transduction in relation to the aetiology using pathological

specimens or cell lines.

A *BRAF* mutation, showing valine to glutamic acid substitution at codon 600 (V600E), is present in 40-60% of ameloblastoma cases with mutation-dependent mitogen-activated protein kinase (MAPK) pathway activation [6-9]. Additionally, several studies have described cases of patients with a *BRAF* V600E mutant that were successfully treated with BRAF inhibitors [10-12], suggesting that *BRAF* V600E signaling might be involved in the development of ameloblastoma. However, the details of the MAPK pathway-dependent mechanism through which ameloblastoma develops are poorly understood.

ADP-ribosylation factor (ARF)-like proteins (ARLs) are a subgroup of ARF small GTP-binding protein superfamily [13]. Recent studies have shown that ARL4C, a member of ARL family proteins, is a target molecule induced by the activation of the RAS- MAPK pathway and Wnt/β-catenin signaling and it plays an important role in both epithelial morphogenesis and tumorigenesis [14-18]. For instance, ARL4C is expressed in some epithelial rudiments, including tooth buds, hair follicles, salivary glands and kidneys, of E15 mouse embryos [14]. The particularly high expression of ARL4C in the distal tip of ureteric buds (UBs) of the mouse embryonic kidney, due to the FGF-RAS-MAPK pathway and Wnt/β-catenin signaling activation, was shown to be involved in UB branching morphogenesis [14].

In contrast, the effects of ARL4C on epithelial tooth bud morphogenesis, which has the same origin as ameloblastoma, remain unclear. ARL4C expression is also upregulated in cancers and associated with the progression of tumorigenesis, including colorectal, lung, tongue, liver, gastric, renal cell, ovarian cancers and glioblastoma [15-17,19-22]. ARL4C expression was reportedly induced in lung premalignant lesions and the exogenous expression of ARL4C promoted cell proliferation of human immortalized

small airway epithelial cells [18], indicating proliferative capabilities of ARL4C, even in premalignant lesions. However, neither ARL4C expression in ameloblastoma nor the effects of its signaling on ameloblastoma development are well understood.

Herein, we found an elevated expression of ARL4C in ameloblastoma cell lines and pathological specimens and demonstrated the role of ARL4C in regulating ameloblastoma cellular growth and ameloblastoma-mediated osteoclast formation.

MATERIALS AND METHODS

Patients and immunohistochemistry

Human ameloblastoma (n=38) tissues were obtained from patients who visited at the Department of Oral and Maxillofacial Surgery, Kyushu University Hospital in the last 10 years (from December 2008 to September 2019), who were diagnosed with ameloblastoma or ameloblastoma, unicystic type according to the recent WHO Classification [1], and who underwent surgery. The clinicopathological data of the patients with ameloblastoma are presented in supplementary material, Table S1. The study protocol was approved by the ethical review board of the Local Ethical Committee of Kyushu University, Japan (#29-392). Resected specimens were macroscopically examined to determine the location and size of ameloblastoma, and histological specimens were fixed in 10% (v/v) formalin and processed for paraffin embedding. Specimens were sectioned (thickness: 4 μm) and stained with hematoxylin-eosin (H&E) for independent evaluation by three pathologists.

Immunohistochemical staining was performed as previously described [23,24]. See supplementary Materials and methods for further details.

Cells and reagents

AM-1 human ameloblastoma cells were kindly provided from Dr. H. Harada (Iwate Medical University, Shiwa-gun, Japan) [25]. AB10 and ABSV, primary ameloblastoma cells, and HeLaS3 human uterine cancer cells, A549 human lung adenocarcinoma cells and NCI-H520 human lung squamous cell carcinoma cells were used in the previous study [6,15,16]. Lenti-X™ 293T (X293T) cells were purchased from Takara Bio Inc. (Shiga, Japan). AM-1 cells were cultured in Keratinocyte SFM medium (Invitrogen,

Carlsbad, CA, USA). AB10 and ABSV were cultured in CnT-PR medium (CELLnTEC, Bern, Switzerland). HeLaS3, A549 and X293T cells were grown in Dulbecco's modified Eagle's medium (Invitrogen) supplemented with 10% FBS (Invitrogen). NCI-H520 cells were grown in RPMI-1640 (Invitrogen) supplemented with 10% FBS. See supplementary Materials and methods.

Plasmid construction and infection using lentivirus harboring a cDNA

Lentiviral vectors were constructed by subcloning GFP, pEGFPN3-ARL4C and ARF6^{Q67L} cDNAs into CSII-CMV-MCS-IRES2-Bsd (kindly provided by Dr. H. Miyoshi (RIKEN BioResource Center, Ibaraki, Japan) [14,26]. The vectors were then transfected with the packaging vectors, pCAG-HIV-gp and pCMV-VSV-G-RSV-Rev, into X293T cells using Lipofectamine LTX reagent (Invitrogen) to generate lentiviruses [27]. See supplementary Materials and methods for further details.

Knockdown of protein expression by siRNA and quantitative RT-PCR

The effects of protein knockdown by siRNA were analyzed as previously described [28]. Briefly, siRNAs (final conc. 20 nM) were transfected into AM-1 cells using Lipofectamine RNAiMAX (Invitrogen). The target sequences are listed in supplementary material, Table S2. The transfected cells were then used for experiments conducted at 48 h post-transfection.

Quantitative RT-PCR was performed as previously described [29]. The primers are listed in supplementary material, Table S3.

Generation of *ARL4C* knockout cells

The target sequence for human *ARL4C*, 5'-CTTCTCGGTGTTGAAGCCGA-3', was designed with the help of CRISPR Genome Engineering Resources (http://www.genome-engineering.org/crispr/) [30]. The plasmids, which were pX330 expressing hCas9 and single-guide RNA (sgRNA) targeting ARL4C and Blasticidin resistance, were transfected into AM-1 cells using Lipofectamine LTX reagent and the transfected cells were selected in medium containing 5 μg/mL Blasticidin S (FUJIFILM Wako, Osaka, Japan) [16]. Single colonies were picked, mechanically disaggregated, and replated into individual wells of 24-well plates.

Osteoclast formation

Mouse primary osteoblasts (POBs) were obtained from the calvaria of newborn C57B16/J mice (Jackson Laboratory, Bar Harbor, ME, USA) by a conventional method using collagenase, as previously described [31]. Mouse bone marrow cells (BMCs) (2×10^6 cells) were isolated from 6-week-old C57B16/J mice and co-cultured with the POBs (1×10^4 cells) in 0.225 ml of α-MEM containing 10% FBS and 0.075 ml of Keratinocyte SFM in 48-well plates. Then, AM-1 cells (2×10^4 cells) were added to the coculture system. After 7 days, the cells were fixed and stained for tartrate-resistant acid phosphatase (TRAP). TRAP-positive cells were counted as osteoclast-like cells. The bone-resorbing activity of osteoclasts was assessed using an Osteo Assay Plate (Corning, Corning, NY, USA).

Statistical analysis

Statistical analyses were performed using JMP Pro 15 software. Significant differences were determined using Fisher's exact test for clinicopathological analyses. For other

experiments, significant differences were determined using Student's *t*-test and one-way ANOVA with Tukey's test. A P value of <0.05 was considered to indicate statistical significance.

Additional Assays

Cell proliferation and migration assays were performed as previously described [29,32]. Western blotting data were representative of at least three independent experiments.

RESULTS

ARL4C is expressed in human ameloblastoma tissue

Immunohistochemical analyses were carried out to examine the ARL4C expression in human ameloblastoma specimens. Clinicopathologically, no significant differences were observed between conventional and unicystic ameloblastomas, regarding sex, location, size or recurrence (supplementary material, Table S1). Cytoplasmic staining for ARL4C was observed in 28 (73.7%) of 38 tumour cases, whereas it was hardly detected in adjacent oral non-tumourous stratified squamous cell regions consistent with a previous report (Figure 1) [16]. The results were considered positive when >40% of the total epithelial cells within a single specimen were stained with anti-ARL4C antibody. Interestingly, ARL4C was strongly expressed in the tumour cells invading the surrounding stroma (Figure 1; black arrowheads). No association was found between ARL4C expression and location, sex, size or recurrence (Table 1). The positive rates of ARL4C staining were lower in the ameloblastoma, unicystic type (2/7; 28.6%) than in the ameloblastoma (26/31; 74.3%) (p<0.01; Fisher's exact test) (Figure 1), suggesting that the expression of ARL4C might be related to the ameloblastoma subtypes.

RAF1-dependent ARL4C expression is required for ameloblastoma cell proliferation

Since ARL4C is efficiently transcribed by the simultaneous activation of RAS-MAPK pathway and Wnt/β-catenin signaling [14,15], we examined the molecular mechanism by which ARL4C expression is induced in ameloblastoma using AM-1 cells, an ameloblastoma cell line harboring a *BRAF* V600E mutation [8]. ARL4C expression in AM-1 cells was comparable to that in A549, SAS and NCI-H520 cells, wherein the

elevated expression of ARL4C is involved in tumorigenesis [15,16] (Figure 2A). β-Catenin siRNA and PD168393 (a selective EGFR inhibitor) did not affect the ARL4C expression, but the simultaneous inactivation of the EGFR pathway and β-catenin signaling reduced ARL4C (supplementary material, Figure S1A).

As *BRAF* V600E-dependent MAPK activation regulates ameloblastoma cell proliferation, we examined the effects of MAPK activation on ARL4C expression in AM-1 cells. The inhibition of the MAPK pathway by PD184161 (a selective MEK1/2 inhibitor) suppressed ERK1/2 activation and reduced the ARL4C expression (Figure 2B), suggesting that ARL4C is dependent on MEK/ERK activation in AM-1 cells. Surprisingly, BRAF V600E inhibitors SB590885, Dabrafenib or Vemurafenib reduced ERK activation but did not affect ARL4C expression (Figure 2B and supplementary material, Figure S1B). In addition, BRAF knockdown did not reduce ARL4C expression (Figure 2C and supplementary material, Figure S1C), suggesting that ARL4C might depend on another MEK/ERK pathway, besides the BRAF V600E-dependent MEK/ERK pathway, in AM-1 cells.

BRAF reportedly forms a complex with wild-type RAF1 (also known as C-RAF) and then increases RAF1 kinase activity, thereby stimulating the MEK/ERK pathway [33,34]. Therefore, we examined the effect of RAF1 on ARL4C expression in AM-1 cells. Raf1 Kinase Inhibitor I suppressed ERK1/2 activation and the ARL4C expression (Figure 2B and supplementary material, Figure S1D). Treatment with SB590885 further reduced ARL4C expression, which was partially decreased by treatment with low concentrations of Raf1 kinase inhibitor I (supplementary material, Figure S1E). The results were consistent with the findings that BRAF V600E activates RAF1 kinase activity [33]. Furthermore, RAF1 knockdown decreased ARL4C expression (Figure 2C and

supplementary material, Figure S1C). *RAF1* expression in AM-1 cells was higher than that in HeLaS3, A549, SAS or NCI-H520 cells (Figure 2D). Immunohistochemically, RAF1 expression in ameloblastoma was higher than in adjacent oral non-tumourous stratified squamous cell regions (Figure 2E), suggesting that ARL4C expression may depend on RAF1-MEK/ERK pathway in AM-1 cells. Additionally, early growth response 1 (*EGR1*), FOS like 1, AP-1 transcription factor subunit (*FOSL1*), cyclin D1 (*CCND1*) and MYC proto-oncogene, bHLH transcription factor (*C-Myc*) were down-regulated by treatment with PD184161 or Raf1 Kinase Inhibitor I (supplementary material, Figure S1F). However, the *CCND1* and *C-Myc* levels were not regulated by treatment with SB590885, indicating that *CCND1* and *C-Myc* as well as ARL4C were not downstream of the BRAF V600E-dependent MEK/ERK pathway.

Next, we assessed the ARL4C expression patterns with BRAF V600E and/or RAF1 in ameloblastoma specimens. Immunohistochemical data revealed that BRAF V600E expression was detected in 25 (65.8%) of 38 tumour lesions, but not in non-tumour regions, consistent with previous reports [6,8,9,35] (Figure 2F and Table 2). ARL4C was detected along with the expression of BRAF V600E in 19 of 38 (50%) (Table 2). However, RAF1 expression was clearly and frequently detected in the cytoplasm of the tumour cells (31/38; 81.6%), immunohistochemically (Figure 2F and Table 2). ARL4C-positive cases, which were co-expressed with RAF1, were 24/38 (63.2%). ARL4C-positive cases, which were co-expressed with both BRAF V600E and RAF1, were 19/38 (50%) (Table 2). Importantly, tumours that were double-positive for BRAF V600E and RAF1 were more frequent (19/28; 67.9%), but not significantly, in ARL4C-positive cases than in ARL4C-negative cases (Figure 2F; lower panel). Conversely, only 4/38 (10.5%) ARL4C-positive cases were negative for both RAF1 and BRAF V600E (Table 2). These data suggest that

ARL4C expression might be regulated by not only *BRAF* V600E mutations but also by RAF1 expression in ameloblastoma. No association was found between the expression levels of RAF1 or BRAF V600E and the ameloblastoma subtypes or location, size and recurrence; however, the rates of RAF1 and BRAF V600E positivity were higher in women (RAF1: $p<0.05$ and BRAF V600E: $p<0.05$; Fisher's exact test) (supplementary material, Figure S1G and Table S1).

Primary ameloblastoma cells, AB10 cells and ABSV cells, in which ABSV cells harbor a *BRAF* V600E mutation, highly expressed *ARL4C* and *RAF1*, and *ARL4C*; this was dependent on the RAF1 pathway in AB10 cells (Figure 2G and supplementary material, Figure S1H). These data indicated that the RAF1-MEK/ERK pathway induces ARL4C expression, not only in immortalized ameloblastoma cells, but also in primary ameloblastoma cells.

Loss-of-function experiments using siRNAs and an inhibitor also revealed that RAF1 expression and its activation are involved in AM-1 cell proliferation (Figure 3A). Additionally, SB590885 reduced the cell proliferation capabilities of AM-1 cells (supplementary material, Figure S2A), and simultaneous inhibition combined with Raf1 Kinase Inhibitor I further suppressed cellular growth (Figure 3B), suggesting that the RAF1-MEK/ERK and BRAF V600E-MEK/ERK pathways might regulate AM-1 cell proliferation independently.

To elucidate the role of RAF1-dependent ARL4C expression in AM-1 cell proliferation, we generated stably ARL4C expressing cells. Then, lentiviral transduction with ARL4C-GFP rescued the Raf1 kinase inhibitor-dependent reduction in ARL4C protein expression and loss-of-function experiments-dependent decreased cellular growth (Figure 3C and 3D), suggesting that RAF1-dependent ARL4C expression may promote ameloblastoma

cell proliferation. Cells expressing ARL4C-GFP showed similar proliferation capabilities to control cells expressing GFP (Figure 3C), suggesting that the endogenous ARL4C expression sufficiently regulates the proliferative ability. SB590885 reduced proliferation capabilities of AM-1 cell expressing not only GFP but also ARL4C-GFP (supplementary material, Figure S2B), supporting the hypothesis that RAF1-MEK/ERK-ARL4C and BRAF V600E-MEK/ERK pathways might regulate AM-1 cell proliferation independently.

ARL4C expression is involved in the proliferation and migration of ameloblastoma cells

ARL4C expression was shown to be involved in the proliferation and migration of colon cancer, lung cancer and tongue cancer cells [15,16]. To elucidate the functions of ARL4C in AM-1 cells, ARL4C was knocked down by two different siRNAs (supplementary material, Figure S3A). ARL4C knockdown decreased migration capability of AM-1 cells (supplementary material, Figure S3B). Because we used ARL4C #1 siRNA, which targets the 3'-UTR (untranslated region) (see supplementary material, Table S2), it did not decrease the amount of exogenously expressed ARL4C-GFP in the cells (supplementary material, Figure S3C). Subsequent ARL4C-GFP expression rescued the ARL4C-knockdown phenotype of tumour cells, excluding siRNA off-target effects (supplementary material, Figure S3D).

To further examine the effect of ARL4C on cell proliferation, ARL4C-knockout AM-1 cells were generated using a CRISPR/Cas9 system (supplementary material, Figure S4A). Genomic deletion and the complete loss of ARL4C protein in the knockout cells were confirmed (Figure 4A and supplementary material, Figure S4B). ARL4C knockout

suppressed proliferation and migration capabilities of AM-1 cells (Figure 4B and supplementary material, Figure S4C). As the ARNO-ARF6 pathway can act downstream of ARL4C to regulate tube formation in intestinal epithelial cells [14] and gene expression in hepatocellular carcinoma [17], we examined whether its pathway could affect the growth potential of AM-1 cells. Treatment with SecinH3 (an inhibitor of ARNO) reduced the cell proliferation capabilities of AM-1 cells (Figure 4C), and its simultaneous inhibition in combination with SB590885 further suppressed cellular growth (Figure 4D). Furthermore, ARF6^{Q67L} (an active ARF6 mutant) [36] rescued ARL4C-knockout- and/or Raf1 Kinase Inhibitor I-dependent decreased cellular growth (Figure 4E), suggesting that RAF1-MEK/ERK-ARL4C-ARNO-ARF6 signaling might be involved in AM-1 cell proliferation.

ARL4C expression in ameloblastoma induces osteoclast formation

Patients with ameloblastoma often exhibit extensive jaw resorption, which is a common clinical problem. Osteoclasts, multinucleated cells (MNCs) that show TRAP activity, are responsible for bone resorption [37,38]. Therefore, we examined whether or not ARL4C expression in ameloblastoma might induce osteoclast formation. H&E-stained ameloblastoma sections showed that numerous MNCs were aligned on the surface of resorbed bone (Figure 5A and supplementary material, Figure S5). Immunohistochemically, MNCs were positive for Cathepsin K (Figure 5B), indicating that the MNCs in the sections are osteoclasts [39]. In our cases (n=28), ameloblastoma cells expressing ARL4C appeared to be separated from osteoclasts at a distance of 678.13 ± 51.49 μm (Figure 5A and supplementary material, Figure S5), suggesting that ameloblastoma may induce osteoclast formation indirectly. The number of osteoclasts in

the ARL4C-positive section was more than that in the ARL4C-negative section, suggesting that ARL4C expression may affect osteoclast formation in ameloblastoma (Figure 5C).

To evaluate the involvement of ameloblastoma in osteoclast formation, AM-1 cells expressing GFP or ARL4C-GFP were co-cultured with mouse BMCs and POBs; thus a few TRAP-positive MNCs and many TRAP-positive mononuclear cells were observed (Figure 6A). However, while MNCs and resorption pits on Osteo Assay Plate were indeed observed (supplementary material, Figure S6A and S6B), co-culture with Keratinocyte SFM medium for AM-1 cells greatly suppressed the number and the size of MNCs compared to the culture with only α-MEM medium (data not shown). Here, TRAP-positive cells were counted as osteoclast-like cells. Then, AM-1 cells induced TRAP-positive cells, and the ARL4C expression further increased the number of TRAP-positive cells (Figure 6A).

Several factors, such as the receptor activator of the NF-κB ligand (RANKL; *Tnfsf11*), its receptor (RANK; *Tnfrsf11a*) and its decoy receptor osteoprotegerin (OPG; *Tnfrsf11b*), are reportedly required for osteoclastogenesis [38,40]. Because the RANKL/RANK pathway regulates osteoclast differentiation, the balanced expression of RANKL and OPG is considered critical for regulating osteoclast function. AM-1 cells dramatically induced mouse *Tnfs11* expression and reduced mouse *Tnfsf11b* expression in mouse BMCs and/or POBs using mouse-specific primers (Figure 6A; lower panels). ARL4C expression further upregulated the mouse *Tnfsf11* mRNA levels (Figure 6A; lower panels). The *TNFSF11* and *TNFRSF1B* expression in AM-1 cells was comparable to that in HeLaS3, A549, SAS and NCI-H520 cells (supplementary material, Figure S6C). ARL4C expression slightly, but significantly, upregulated human *TNFSF11* mRNA

expression in human AM-1 cells using human-specific primers (supplementary material, Figure S6D). However, a few TRAP-positive cells were observed in the co-culture with BMCs and AM-1 cells expressing ARL4C-GFP in the absence of POBs (data not shown), indicating that the amount of RANKL expressed by AM-1 cells might not be sufficient to induce osteoclastogenesis directly. In the co-culture with BMCs, POBs and AM-1 cells expressing ARL4C-GFP, neutralizing antibodies specific to mouse RANKL, but not human RANKL, reduced the number of TRAP-positive cells (Figure 6B). Therefore, RANKL expression of POBs induced by AM-1 cells expressing ARL4C-GFP may lead to up-regulation of osteoclast formation. Treatment with Raf1 Kinase Inhibitor I or PD184161 suppressed *ARL4C* expression in AM-1 and the number of TRAP-positive cells (Figure 6C and supplementary material, Figure S6E). Finally, ARL4C-knockout AM-1 cells reduced the number of TRAP-positive cells and mouse *Tnfs11* mRNA expression (Figure 6D). Collectively, these results indicated that ameloblastoma cells indirectly promoted osteoclast formation by regulating the balance of RANKL and OPG in osteoblasts/stromal cells, and that the RAF1-MEK/ERK-dependent expression of ARL4C might be involved in the regulation of this balance.

DISCUSSION

Recent studies have highlighted various gene mutations related to the MAPK pathway, including *FGFR2*, *BRAF*, *KRAS*, *NRAS* and *HRAS*, in ameloblastoma, with *BRAF* V600E being the most common (40-60%) [6,8,9,35], suggesting that *BRAF* V600E mutations may be involved in the aetiology of ameloblastoma development.

Consistently, our immunohistochemical analyses demonstrated that the expression of BRAF V600E, which coincided 100% with the molecular detection of *BRAF* V600E mutations [8], was observed in 25 (65.8%) of 38 cases. *BRAF* V600E mutations are present in numerous malignant tumours, including melanoma, hairy cell leukemia, papillary thyroid carcinoma and colorectal cancer [34,41-44], and these mutations induce MEK/ERK activation, which is involved in tumorigenesis [45]. Previously, a heterozygous *BRAF* V600E mutation was detected in ameloblastoma specimens and cell lines [6,8,9,35]. Therefore, *BRAF* V600E mutations in ameloblastoma might be associated with lower oncogenic potential compared to malignant tumours harboring homozygous mutations. Notably, BRAF V600E positivity accompanied by ARL4C and RAF1 negativity was seen in only 1 of 38 cases (2.6%) (see Table 2), suggesting that *BRAF* V600E mutations alone may not be sufficient to induce ameloblastoma. Similarly, *BRAF* V600E mutations were observed in 39 (89%) of 44 human cases of benign nevi, indicating that BRAF activation alone is not sufficient for the development of melanoma [46]. Another molecular mechanism besides heterozygous *BRAF* V600E mutation may be involved in the development of ameloblastoma.

ARL4C was highly expressed with RAF1 and BRAF V600E in the lesional tissue of ameloblastoma specimens. The RAF1-MEK/ERK pathway and BRAF V600E-MEK/ERK pathways may cooperatively induce the expression of ARL4C in

ameloblastoma. The current loss-of-function experiments using inhibitors or siRNAs demonstrated that RAF1-MEK/ERK-ARL4C-ARNO-ARF6 pathway and BRAF V600E-MEK/ERK pathway independently promote AM-1 cell proliferation. Collectively, these results support the idea that their combined signal inhibition may be an effective antitumour therapeutic strategy for patients with ameloblastoma. ARL4C reportedly contributes to oncogenesis through its overexpression by multiple mechanisms in a cell-context-dependent manner [15-17]. In ameloblastoma cells, ARL4C expression was shown to depend on RAF1-MEK/ERK pathway (see Figure 2B), suggesting that the RAF1-MEK/ERK pathway may be activated in ameloblastoma.

The overexpression of RAF1 has been observed in various cancers, such as lung adenocarcinomas and multiple myeloma [47,48], suggesting that its overexpression may be associated with tumorigenesis. RAF1 expression was clearly elevated in ameloblastoma cell lines and specimens (see Figure 2D and 2E). Cancer samples bearing *BRAF* V600E mutants did not contain *RAS* mutations [34,43], indicating their exclusive relationship. However, wild-type BRAF forms a complex with RAF1 and then increases RAF1 kinase activity, thereby stimulating the MEK/ERK pathway [33]. Although the definitive mechanisms by which the BRAF V600E-MEK/ERK pathway alone did not affect the expression of ARL4C remain unclear, two hypotheses are proposed. First, so-called paradoxical MAPK activation due to BRAF inhibitor-mediated homodimerization and heterodimerization of wild-type BRAF or RAF1 [49] leads to the secondary activation of the RAF1-MEK/ERK pathway, thereby maintaining the ARL4C expression. Second, the contribution of BRAF V600E to MEK-ERK pathway activation may be relatively low. Thus, it is possible that BRAF V600E is not sufficient to induce ARL4C expression in the presence of RAF1 overexpression, because the complex formation of

BRAF V600E and RAF1 inhibits the kinase activity of BRAF V600E and ERK activation [50]. It is therefore intriguing to speculate that cooperative activation of BRAF V600E and RAF1 would be the aetiology of ameloblastoma cell proliferation and that such cooperative activation might induce the clinical aggressiveness of ameloblastoma beyond the category with benign neoplasia.

While some reports have shown that RANKL, which is secreted by ameloblastoma cells, induces osteoclastogenesis [51,52], ameloblastoma cells appeared to be located separately from osteoclasts in ameloblastoma specimens. We thus hypothesized that ameloblastoma cells induce osteoclast formation indirectly. In support of this, the role of stromal cells has been emphasized in the osteoclastogenesis of patients with ameloblastoma [53]. In the current co-culture system, ameloblastoma cells induced *Tnfsf11* expression and reduced *Tnfrsf11b* expression in mouse BMCs and/or POB, indicating that the interaction of tumour cells and stromal cells/osteoblasts plays a pivotal role in ameloblastoma mediated-osteoclast formation. Although the precise mechanism underlying the upregulation of RANKL or the mechanism of OPG downregulation by AM-1 was unclear, our findings were consistent with previous findings that oral squamous cells induced osteoclast formation by increasing the RANK/OPG ratio of osteoblasts/stromal cells through interaction with osteoblasts/stromal cells [31].

In summary, we found that ARL4C is highly expressed in ameloblastoma specimens with high frequencies and in ameloblastoma cell lines. We also demonstrated that the RAF1-MEK/ERK pathway induces ARL4C expression to regulate ameloblastoma cellular growth positively and promote ameloblastoma-mediated osteoclast formation (supplementary material, Figure S6F). Therefore, these results suggest that the RAF1-MEK/ERK-ARL4C axis contributes to the development of ameloblastoma.

Acknowledgments

The authors thank Drs. K. Nagata, T. Harada, Y. Kami, H. Hiura, Y. Tajiri, K. Hasegawa, R. Nagano, S. Nakamura, Y. Mori and H. Wada for valuable technical support in this research. The authors also thank the Research Support Center, Graduate School of Medical Sciences, Kyushu University. We appreciate the technical assistance from The Joint Use Laboratories, Faculty of Dental Science, Kyushu University. This work was supported by JSPS KAKENHI Grants to S. F. (2020-2022) (20K09906) and T. K. (2020-2022) (20K10096), Fukuoka Foundation for Sound Health Cancer Research Fund, Takeda Science Foundation, The Shin-Nihon Foundation of Advanced Medical Research and SGH Foundation to S.F. and Maritza ja Reino Salonen Foundation to K.H.

Author contributions

S. F. carried out experiments, conceived and wrote the manuscript. T. I. carried out immunohistochemical experiments and co-wrote the manuscript. M. K. carried out ARL4C expression experiments and clinicopathological analyses. T. F. and S. S. analyzed immunohistochemical data. S. M. and A. K. interpreted the data and co-wrote the manuscript. E. J. carried out osteoclast formation experiments. K. K., J. P., J. C., P. M., K. H. established primary ameloblastoma cells and interpreted the data. T. K. carried out data interpretation and co-wrote the manuscript. All authors were involved in writing the paper and had final approval of the submitted and published versions.

Supporting Information

Supplementary figure legends

Figure S1. ARL4C expression depends on RAF1-MEK/ERK pathway in ameloblastoma.

Figure S2. The effect of BRAF V600E signaling on the proliferation of ameloblastoma cells.

Figure S3. ARL4C expression is involved in the migration of ameloblastoma cells.

Figure S4. Generation of ARL4C knockout cells.

Figure S5. ARL4C expression in ameloblastoma tissues.

Figure S6. ARL4C expression in ameloblastoma induces osteoclast formation.

Table S1. The clinicopathological data of the patients with ameloblastoma.

Table S2. List of siRNAs sequence used in this study.

Table S3. List of quantitative RT-PCR primers used in this study.

References

1. Vered M, Muller S, Heikinhemio K. Ameloblastoma. Benign epithelial odontogenic tumours. In WHO classification of head and neck tumours, (4th edn), El-Naggar AK,Chan JKC, Grandis JR, *et al.* (eds). IARC: Lyon, 2017; 215-218.
2. Mendenhall WM, Werning JW, Fernandes R*, et al.* Ameloblastoma. *Am J Clin Oncol* 2007; **30**: 645-648.
3. Heikinheimo K, Huhtala JM, Thiel A*, et al.* The Mutational Profile of Unicystic Ameloblastoma. *J Dent Res* 2019; **98**: 54-60.
4. Mano H. Cancer genomic medicine in Japan. *Proc Jpn Acad Ser B Phys Biol Sci* 2020; **96**: 316-321.
5. Buchner A, Merrell PW, Carpenter WM. Relative frequency of central odontogenic tumors: a study of 1,088 cases from Northern California and comparison to studies from other parts of the world. *J Oral Maxillofac Surg* 2006; **64**: 1343-1352.
6. Kurppa KJ, Caton J, Morgan PR*, et al.* High frequency of BRAF V600E mutations in ameloblastoma. *J Pathol* 2014; **232**: 492-498.
7. Sweeney RT, McClary AC, Myers BR*, et al.* Identification of recurrent SMO and BRAF mutations in ameloblastomas. *Nat Genet* 2014; **46**: 722-725.
8. Brown NA, Rolland D, McHugh JB*, et al.* Activating FGFR2-RAS-BRAF mutations in ameloblastoma. *Clin Cancer Res* 2014; **20**: 5517-5526.
9. Seki-Soda M, Sano T, Ito K*, et al.* An immunohistochemical and genetic study of BRAF(V600E) mutation in Japanese patients with ameloblastoma. *Pathol Int* 2020; **70**: 224-230.
10. Tan S, Pollack JR, Kaplan MJ*, et al.* BRAF inhibitor treatment of primary BRAF-mutant ameloblastoma with pathologic assessment of response. *Oral Surg Oral Med Oral Pathol Oral Radiol* 2016; **122**: e5-7.
11. Faden DL, Algazi A. Durable treatment of ameloblastoma with single agent BRAFi Re: Clinical and radiographic response with combined BRAF-targeted therapy in stage 4 ameloblastoma. *J Natl Cancer Inst* 2017; **109**.
12. Fernandes GS, Girardi DM, Bernardes JPG*, et al.* Clinical benefit and radiological response with BRAF inhibitor in a patient with recurrent ameloblastoma harboring V600E mutation. *BMC Cancer* 2018; **18**: 887.
13. Matsumoto S, Fujii S, Kikuchi A. Arl4c is a key regulator of tubulogenesis and tumourigenesis as a target gene of Wnt-β-catenin and growth factor-Ras signalling. *J Biochem* 2017; **161**: 27-35.
14. Matsumoto S, Fujii S, Sato A*, et al.* A combination of Wnt and growth factor

signaling induces Arl4c expression to form epithelial tubular structures. *EMBO J* 2014; **33**: 702-718.

15. Fujii S, Matsumoto S, Nojima S, *et al.* Arl4c expression in colorectal and lung cancers promotes tumorigenesis and may represent a novel therapeutic target. *Oncogene* 2015; **34**: 4834-4844.
16. Fujii S, Shinjo K, Matsumoto S, *et al.* Epigenetic upregulation of ARL4C, due to DNA hypomethylation in the 3'-untranslated region, promotes tumorigenesis of lung squamous cell carcinoma. *Oncotarget* 2016; **7**: 81571-81587.
17. Harada T, Matsumoto S, Hirota S, *et al.* Chemically Modified Antisense Oligonucleotide Against ARL4C Inhibits Primary and Metastatic Liver Tumor Growth. *Mol Cancer Ther* 2019; **18**: 602-612.
18. Kimura K, Matsumoto S, Harada T, *et al.* ARL4C is associated with initiation and progression of lung adenocarcinoma and represents a therapeutic target. *Cancer Sci* 2020; **111**: 951-961.
19. Hu Q, Masuda T, Sato K, *et al.* Identification of ARL4C as a Peritoneal Dissemination-Associated Gene and Its Clinical Significance in Gastric Cancer. *Ann Surg Oncol* 2018; **25**: 745-753.
20. Isono T, Chano T, Yoshida T, *et al.* ADP-ribosylation factor-like 4C is a predictive biomarker of poor prognosis in patients with renal cell carcinoma. *Am J Cancer Res* 2019; **9**: 415-423.
21. Wakinoue S, Chano T, Amano T, *et al.* ADP-ribosylation factor-like 4C predicts worse prognosis in endometriosis-associated ovarian cancers. *Cancer Biomark* 2019; **24**: 223-229.
22. Chen Q, Weng HY, Tang XP, *et al.* ARL4C stabilized by AKT/mTOR pathway promotes the invasion of PTEN-deficient primary human glioblastoma. *J Pathol* 2019; **247**: 266-278.
23. Matsumoto S, Kurimoto T, Taketo MM, *et al.* The WNT/MYB pathway suppresses KIT expression to control the timing of salivary proacinar differentiation and duct formation. *Development* 2016; **143**: 2311-2324.
24. Mikami Y, Fujii S, Kohashi KI, *et al.* Low-grade myofibroblastic sarcoma arising in the tip of the tongue with intravascular invasion: A case report. *Oncol Lett* 2018; **16**: 3889-3894.
25. Harada H, Mitsuyasu T, Nakamura N, *et al.* Establishment of ameloblastoma cell line, AM-1. *J Oral Pathol Med* 1998; **27**: 207-212.
26. Miyoshi H, Blomer U, Takahashi M, *et al.* Development of a self-inactivating lentivirus vector. *J Virol* 1998; **72**: 8150-8157.

27. Hasegawa K, Fujii S, Matsumoto S*, et al.* YAP signaling induces PIEZO1 to promote oral squamous cell carcinoma cell proliferation. *J Pathol* 2021; **253**: 80-93.
28. Mikami Y, Fujii S, Nagata K*, et al.* GLI-mediated Keratin 17 expression promotes tumor cell growth through the anti-apoptotic function in oral squamous cell carcinomas. *J Cancer Res Clin Oncol* 2017; **143**: 1381-1393.
29. Fujii S, Tajiri Y, Hasegawa K*, et al.* The TRPV4-AKT axis promotes oral squamous cell carcinoma cell proliferation via CaMKII activation. *Lab Invest* 2020; **100**: 311-323.
30. Hsu PD, Scott DA, Weinstein JA*, et al.* DNA targeting specificity of RNA-guided Cas9 nucleases. *Nat Biotechnol* 2013; **31**: 827-832.
31. Tada T, Jimi E, Okamoto M*, et al.* Oral squamous cell carcinoma cells induce osteoclast differentiation by suppression of osteoprotegerin expression in osteoblasts. *Int J Cancer* 2005; **116**: 253-262.
32. Fujii S, Nagata K, Matsumoto S*, et al.* Wnt/β-catenin signaling, which is activated in odontomas, reduces Sema3A expression to regulate odontogenic epithelial cell proliferation and tooth germ development. *Sci Rep* 2019; **9**: 4257.
33. Garnett MJ, Rana S, Paterson H*, et al.* Wild-type and mutant B-RAF activate C-RAF through distinct mechanisms involving heterodimerization. *Mol Cell* 2005; **20**: 963-969.
34. Rajagopalan H, Bardelli A, Lengauer C*, et al.* Tumorigenesis: RAF/RAS oncogenes and mismatch-repair status. *Nature* 2002; **418**: 934.
35. Yukimori A, Oikawa Y, Morita KI*, et al.* Genetic basis of calcifying cystic odontogenic tumors. *PLoS One* 2017; **12**: e0180224.
36. Aikawa Y, Martin TF. ARF6 regulates a plasma membrane pool of phosphatidylinositol(4,5)bisphosphate required for regulated exocytosis. *J Cell Biol* 2003; **162**: 647-659.
37. Nakamura I, Takahashi N, Jimi E*, et al.* Regulation of osteoclast function. *Mod Rheumatol* 2012; **22**: 167-177.
38. Takayanagi H. SnapShot: Osteoimmunology. *Cell Metab* 2015; **21**: 502 e501.
39. Tohyama R, Kayamori K, Sato K*, et al.* Establishment of a xenograft model to explore the mechanism of bone destruction by human oral cancers and its application to analysis of role of RANKL. *J Oral Pathol Med* 2016; **45**: 356-364.
40. Boyle WJ, Simonet WS, Lacey DL. Osteoclast differentiation and activation. *Nature* 2003; **423**: 337-342.
41. Curtin JA, Fridlyand J, Kageshita T*, et al.* Distinct sets of genetic alterations in

melanoma. *N Engl J Med* 2005; **353**: 2135-2147.

42. Tiacci E, Trifonov V, Schiavoni G*, et al.* BRAF mutations in hairy-cell leukemia. *N Engl J Med* 2011; **364**: 2305-2315.
43. Davies H, Bignell GR, Cox C*, et al.* Mutations of the BRAF gene in human cancer. *Nature* 2002; **417**: 949-954.
44. Puxeddu E, Moretti S, Elisei R*, et al.* BRAF(V599E) mutation is the leading genetic event in adult sporadic papillary thyroid carcinomas. *J Clin Endocrinol Metab* 2004; **89**: 2414-2420.
45. Niault TS, Baccarini M. Targets of Raf in tumorigenesis. *Carcinogenesis* 2010; **31**: 1165-1174.
46. Pollock PM, Harper UL, Hansen KS*, et al.* High frequency of BRAF mutations in nevi. *Nat Genet* 2003; **33**: 19-20.
47. Cekanova M, Majidy M, Masi T*, et al.* Overexpressed Raf-1 and phosphorylated cyclic adenosine 3'-5'-monophosphatate response element-binding protein are early markers for lung adenocarcinoma. *Cancer* 2007; **109**: 1164-1173.
48. Muller E, Bauer S, Stuhmer T*, et al.* Pan-Raf co-operates with PI3K-dependent signalling and critically contributes to myeloma cell survival independently of mutated RAS. *Leukemia* 2017; **31**: 922-933.
49. Poulikakos PI, Zhang C, Bollag G*, et al.* RAF inhibitors transactivate RAF dimers and ERK signalling in cells with wild-type BRAF. *Nature* 2010; **464**: 427-430.
50. Karreth FA, DeNicola GM, Winter SP*, et al.* C-Raf inhibits MAPK activation and transformation by B-Raf(V600E). *Mol Cell* 2009; **36**: 477-486.
51. Sandra F, Hendarmin L, Kukita T*, et al.* Ameloblastoma induces osteoclastogenesis: a possible role of ameloblastoma in expanding in the bone. *Oral Oncol* 2005; **41**: 637-644.
52. Tay JY, Bay BH, Yeo JF*, et al.* Identification of RANKL in osteolytic lesions of the facial skeleton. *J Dent Res* 2004; **83**: 349-353.
53. Sathi GS, Nagatsuka H, Tamamura R*, et al.* Stromal cells promote bone invasion by suppressing bone formation in ameloblastoma. *Histopathology* 2008; **53**: 458-467.

Table 1. Clinical characteristics of ameloblastoma patients with ARL4C expression.

Categorical variables	ARL4C positive (n = 28)	ARL4C negative (n = 10)
Age	39.9±16.7	34.9±20.9
Location		
Mandible	22 (57.9%)	9 (23.7%)
Maxilla	6 (15.8%)	1 (2.6%)
Sex		
Male	18 (47.4%)	6 (15.8%)
Female	10 (26.3%)	4 (10.5%)
Size		
Mesiodistal×buccolingual ×vertical	37.7±18.5×21.9±9.2 ×27.3±13.5	42.4±17.9×25.4±7.7 ×51.7±29.9
Clinical prognosis		
Primary	24 (63.2%)	6 (15.8%)
Recurrence	4 (10.5%)	4 (10.5%)

Size was calculated by computed tomography scan.

Radiographically, image characteristics of ameloblastoma and ameloblastoma, unicystic type were multilocular and unilocular, respectively.

Table 2. ARL4C, BRAF V600E or RAF1 expression in ameloblastomas.

ARL4C	BRAF V600E	RAF1	Number
-	-	-	2
-	-	+	2
-	+	-	1
-	+	+	5
+	-	-	4
+	-	+	5
+	+	-	0
+	+	+	19

-: Negative, +: Positive

FIGURE LEGENDS

Figure 1. ARL4C is expressed in human ameloblastomas.

Ameloblastoma tissues (n=38) were stained with anti-ARL4C antibody and hematoxylin. Ameloblastoma and ameloblastoma, unicystic type are examined, and ARL4C-positive or -negative cases in each type are shown in the lower panel. Black boxes show enlarged images. Black arrowheads indicate ameloblastoma cells that invade in the stroma. Scale bars, 100 μm.

Figure 2. ARL4C expression depends on RAF1-MEK/ERK pathway in ameloblastoma.

(A) *ARL4C* mRNA levels in HeLaS3, A549, SAS, NCI-H520 and AM-1 cells were measured by quantitative RT-PCR. Relative levels of *ARL4C* mRNA expression were normalized to *GAPDH* and expressed as fold-changes compared with expression in HeLaS3 cells. (B) AM-1 cells were cultured without or with 10 μM PD184161, 10 μM Raf1 Kinase Inhibitor I or 10 μM SB590885 for 24 h. Cell lysates were probed with anti-ARL4C, anti-phospho-ERK1/2, anti-ERK1/2 and anti-β-actin antibodies. (C) AM-1 cells were transfected with control or four independent BRAF or RAF1 siRNAs. Cell lysates were probed with anti-ARL4C and anti-β-actin antibodies. (D) *RAF1* mRNA levels in HeLaS3, A549, SAS, NCI-H520 and AM-1 cells were measured by quantitative RT-PCR. Relative levels of *RAF1* mRNA expression were normalized to *GAPDH* and expressed as fold-changes compared with expression in HeLaS3 cells. (E) Representative ameloblastoma tissue stained with anti-RAF1 antibody, and hematoxylin was shown. Dashed box and solid box indicate enlarged images of oral non-tumourous squamous cell region and ameloblastoma (plexiform type), respectively. (F) Ameloblastoma tissues

(n=38) were stained with anti-ARL4C, anti-RAF1 and BRAF V600E antibodies, and hematoxylin. The numbers of cases with ARL4C-negative or ARL4C-positive, and BRAF V600E- and RAF1-negative or BRAF V600E- and RAF1-positive were shown below. (G) *ARL4C* mRNA levels in HeLaS3, AM-1, AB10 and ABSV cells were measured by quantitative RT-PCR. Relative levels of *ARL4C* mRNA expression were normalized to *GAPDH* and expressed as fold-changes compared with expression in HeLaS3 cells (left panel). AB10 cells were cultured without or with 10 μM Raf1 Kinase Inhibitor I for 24 h. *ARL4C* mRNA levels in AB10 were measured by quantitative RT-PCR. Relative human *ARL4C* mRNA levels were normalized by human *GAPDH* and expressed as fold-changes compared with levels in control cells (right panel). Scale bars, 1 mm (E), 40 μm (F). Results are shown as means ± s.d. of three independent experiments. $*P < 0.01$.

Figure 3. RAF1-dependent ARL4C expression is required for proliferation of ameloblastoma cells.

(A) AM-1 cells were transfected with control or four different RAF1 siRNAs. The cells were cultured for the indicated numbers of days, and cell numbers were counted (left panel). AM-1 cells were cultured without or with 0.1 and 0.5 μM Raf1 Kinase Inhibitor I for the indicated numbers of days, and cell numbers were counted (right panel). (B) AM-1 cells were cultured without or with 0.5 μM Raf1 Kinase Inhibitor I and/or 5 μM SB590885 for the indicated numbers of days, and cell numbers were counted. (C) AM-1 cells expressing GFP or ARL4C-GFP were cultured without or with 1 μM Raf1 Kinase Inhibitor I for 24 h. Cell lysates were probed with anti-ARL4C, anti-phospho-ERK1/2, anti-ERK1/2 and anti-β-actin antibodies (left panels). AM-1 cells expressing GFP or

ARL4C-GFP were cultured without or with 0.5 μM Raf1 Kinase Inhibitor I for the indicated numbers of days, and cell numbers were counted (right panel). (D) AM-1 cells expressing GFP or ARL4C-GFP were transfected with control or RAF1 #1 siRNA. The cells were cultured for the indicated numbers of days, and cell numbers were counted. Results are shown as means ± s.d. of three independent experiments. *$P < 0.01$. **$P < 0.05$.

Figure 4. ARL4C expression is involved in the proliferation of ameloblastoma cells. (A) Lysates of ARL4C knockout AM-1 cells were generated and cell lysates were probed with anti-ARL4C and anti-β-actin antibodies. (B) ARL4C control or knockout AM-1 cells were cultured for the indicated numbers of days, and cell numbers were counted. (C) AM-1 cells were cultured without or with 1, 5 and 10 μM SecinH3 for the indicated numbers of days, and cell numbers were counted. (D) AM-1 cells were cultured without or with 5 μM SecinH3 and/or 5 μM SB590885 for the indicated numbers of days, and cell numbers were counted. (E) ARL4C control or knockout AM-1 cells were transfected with mock or $ARF6^{Q67L}$, and cells lysates were probed with anti-ARF6 and anti-β-actin antibodies (upper panels). ARL4C control or knockout AM-1 cells expressing mock or $ARF6^{Q67L}$ were cultured for the indicated numbers of days, and cell numbers were counted (lower left panel). AM-1 cells expressing mock or $ARF6^{Q67L}$ were cultured without or with 0.5 μM Raf1 Kinase Inhibitor I for the indicated numbers of days, and cell numbers were counted (lower right panel). Results are shown as means ± s.d. of three independent experiments. *$P < 0.01$. **$P < 0.05$.

Figure 5. ARL4C expression in ameloblastoma induces osteoclast formation in the

ameloblastoma tissues.

(A) Ameloblastoma tissues, which were intraosseous, were stained with H&E. Boxes show enlarged images. Black arrowheads and white arrowheads indicate ameloblastoma cells and multinucleated cells, respectively. Dotted lines and black lines indicate the border between ameloblastoma and stroma, and between bone and stroma, respectively. (B) Ameloblastoma tissues, which were intraosseous, were stained with anti-Cathepsin K antibody and hematoxylin. White arrowheads indicate multinucleated cells. Black lines indicate the border between bone and stroma. (C) Representative osteoclasts were shown in the ARL4C-negative or ARL4C-positive specimens. Osteoclasts cell number was counted in the ARL4C-negative or ARL4C-positive specimens (n=22). White arrowheads indicate osteoclasts. Boxes indicate enlarged images. Dotted lines and black lines indicate the border between ameloblastoma and stroma, and between bone and stroma, respectively. Scale bars, 200 μm (A) and 50 μm (B and C). $^{**}P < 0.05$.

Figure 6. ARL4C expression in ameloblastoma induces osteoclast formation indirectly.

(A) AM-1 cells (2×10^4 cells) and mouse BMCs (2×10^6 cells) were co-cultured with POBs (1×10^4 cells) for 7 days in 48-well plates. After the culture, cells were fixed and stained for TRAP (upper left panels), and TRAP-positive cells were counted (upper right panel). Mouse *Tnfsf11* or *Tnfrsf11b* mRNA levels were measured by quantitative RT-PCR. Relative mouse *Tnfsf11* or *Tnfrsf11b* mRNA levels were normalized by mouse *GAPDH* and expressed as fold-changes compared with levels in control cells (lower panels). (B) AM-1 cells and mouse BMCs were co-cultured with POBs without or with neutralizing antibodies to mouse RANKL (10 ng/mL) or human RANKL (10 ng/mL) for

7 days in 48-well plates. After the culture, cells were fixed and stained for TRAP (left panels), and TRAP-positive cells were counted (right panel). (C) AM-1 cells and mouse BMCs were co-cultured with POBs without or with10 μM Raf1 Kinase Inhibitor I or 10 μM PD184161 for initial 2 days and cultured for total 7 days in 48-well plates. After the culture, cells were fixed and stained for TRAP (left panels). Human *ARL4C* mRNA levels were measured by quantitative RT-PCR. Relative human *ARL4C* mRNA levels were normalized by human *GAPDH* and expressed as fold-changes compared with levels in control cells (right panel). (D) ARL4C-knockout AM-1 cells and mouse BMCs were co-cultured with POBs for 7 days in 48-well plates. After the culture, cells were fixed and stained for TRAP (upper left panels), and TRAP-positive cells were counted (upper right panel). Mouse *Tnfsf11* or *Tnfrsf11b* mRNA levels were measured by quantitative RT-PCR. Relative mouse *Tnfsf11* or *Tnfrsf11b* mRNA levels were normalized by mouse *GAPDH* and expressed as fold-changes compared with levels in control cells (lower panels). Results are shown as means ± s.d. of three independent experiments. Scale bars, 200 μm. *$P < 0.01$. **$P < 0.05$.

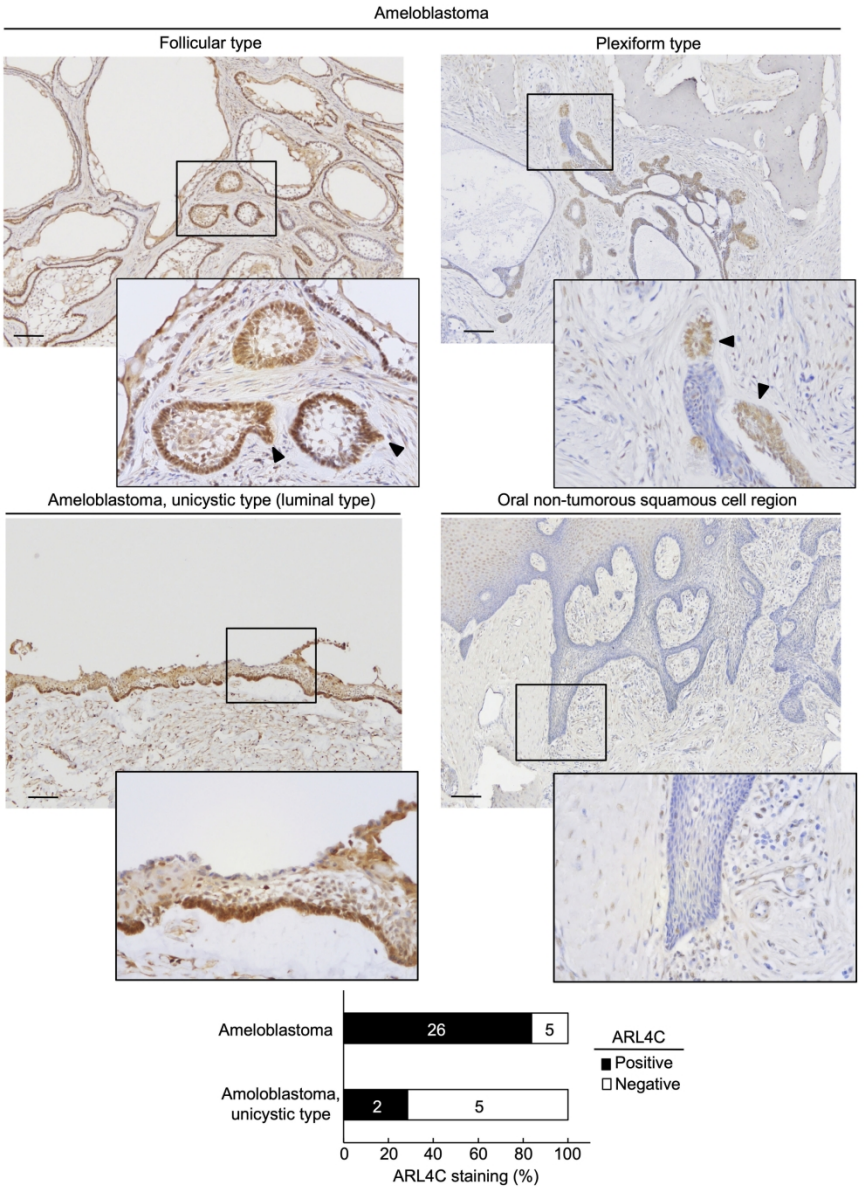

Figure 1: ARL4C is expressed in human ameloblastomas.

190x254mm (300 x 300 DPI)

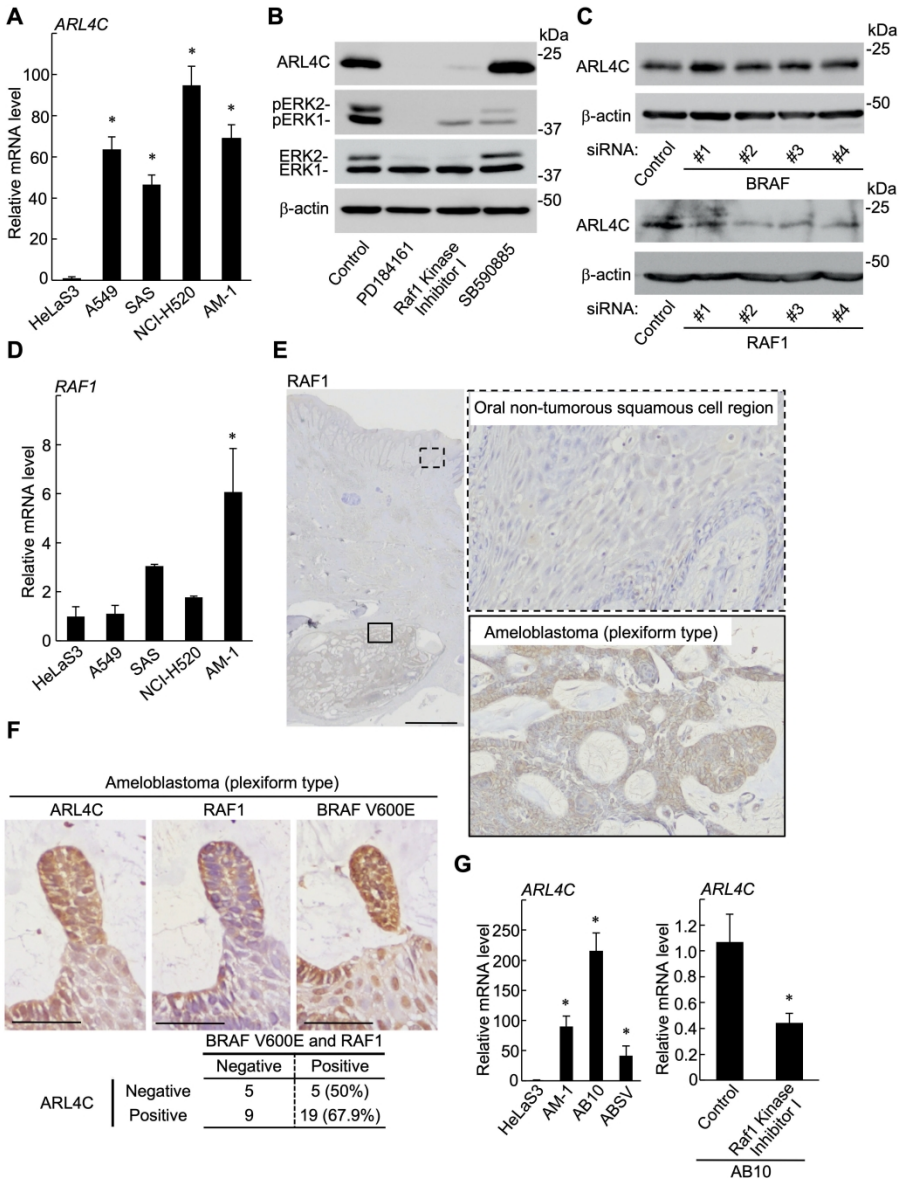

Figure 2: ARL4C expression depends on RAF1-MEK/ERK pathway in ameloblastoma.

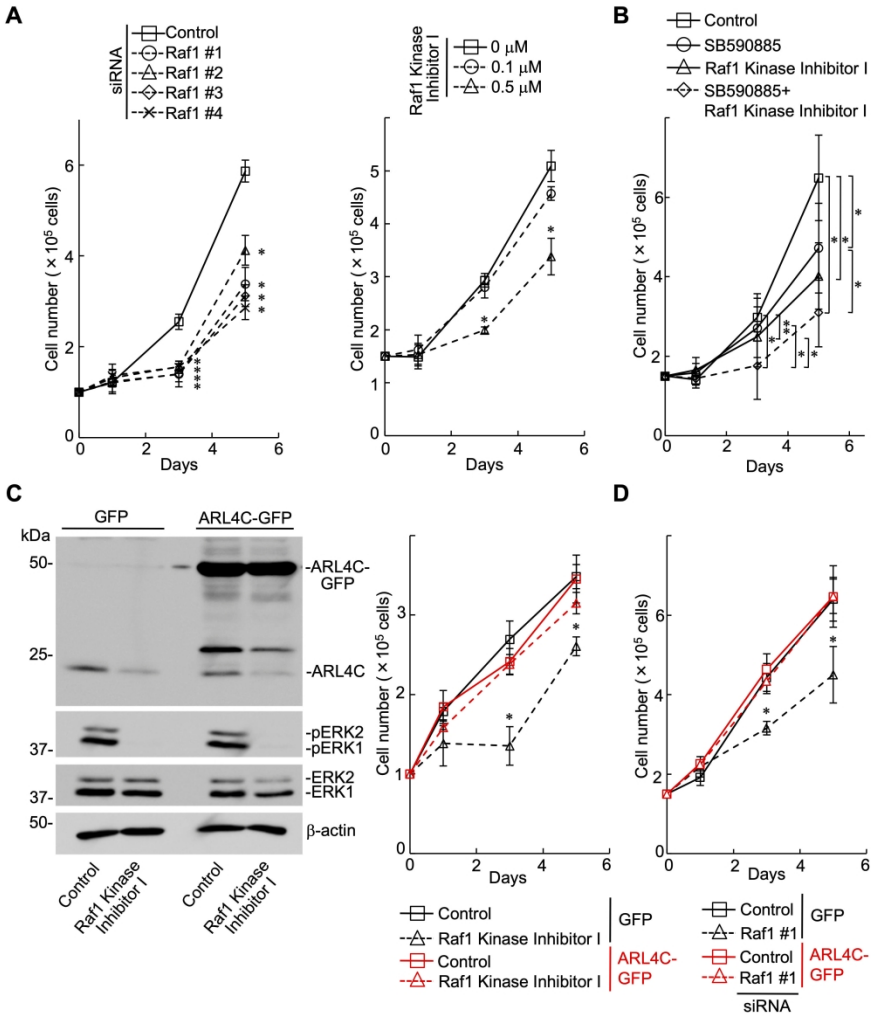

Figure 3: RAF1-dependent ARL4C expression is required for proliferation of ameloblastoma cells.

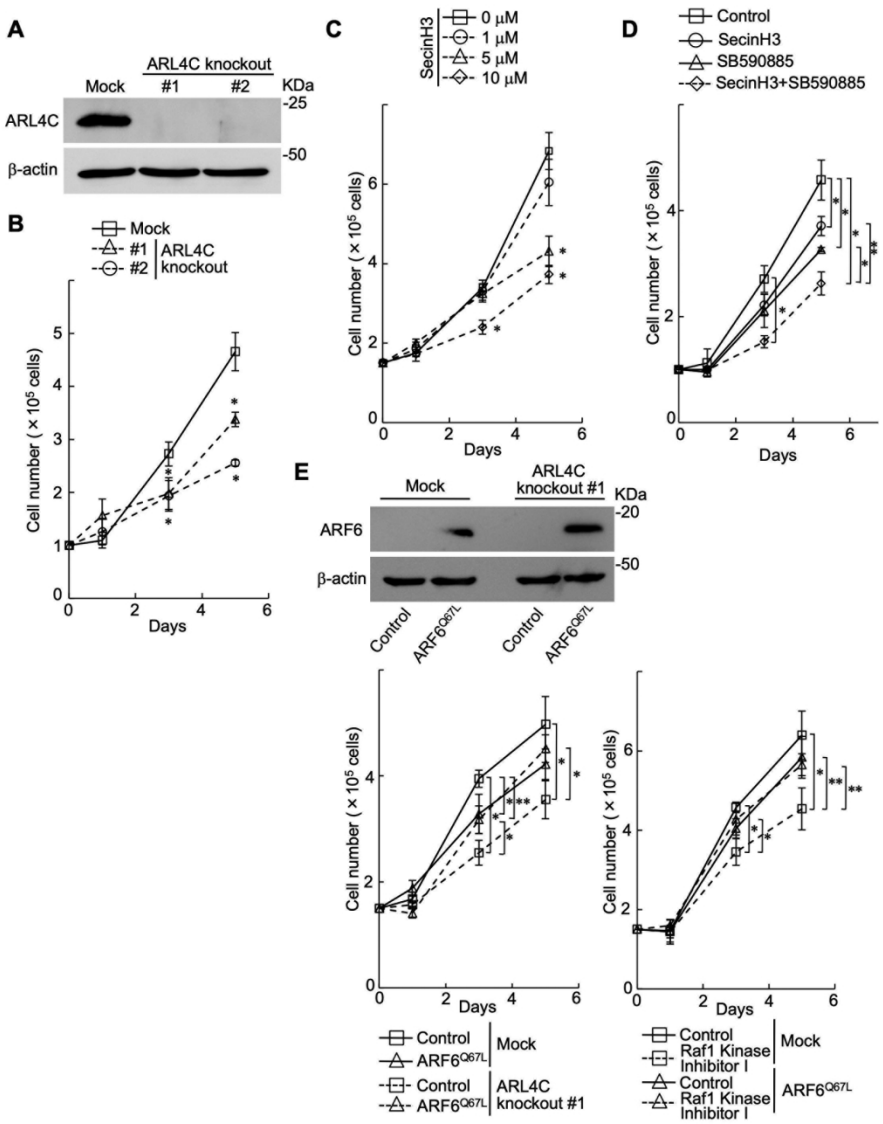

Figure 4: ARL4C expression is involved in the proliferation of ameloblastoma cells.

190x254mm (300 x 300 DPI)

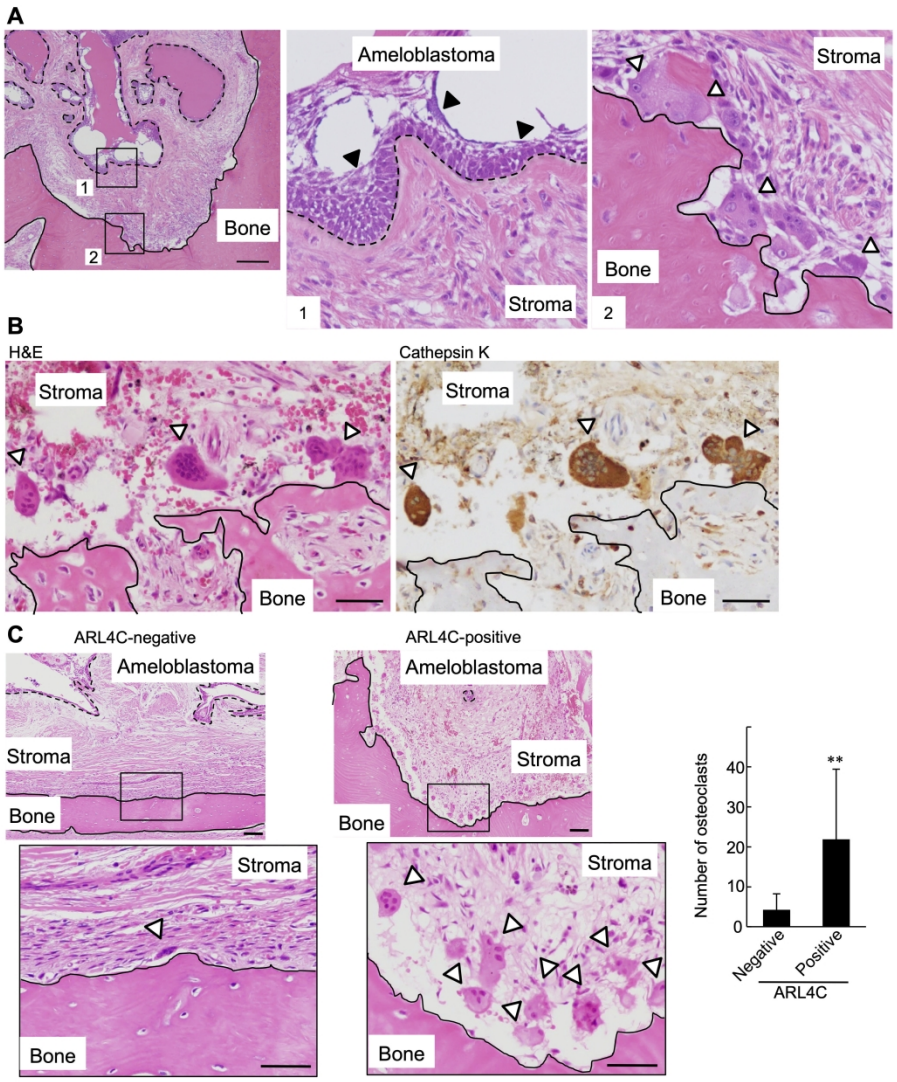

Figure 5: ARL4C expression in ameloblastoma induces osteoclast formation in the ameloblastoma tissues.

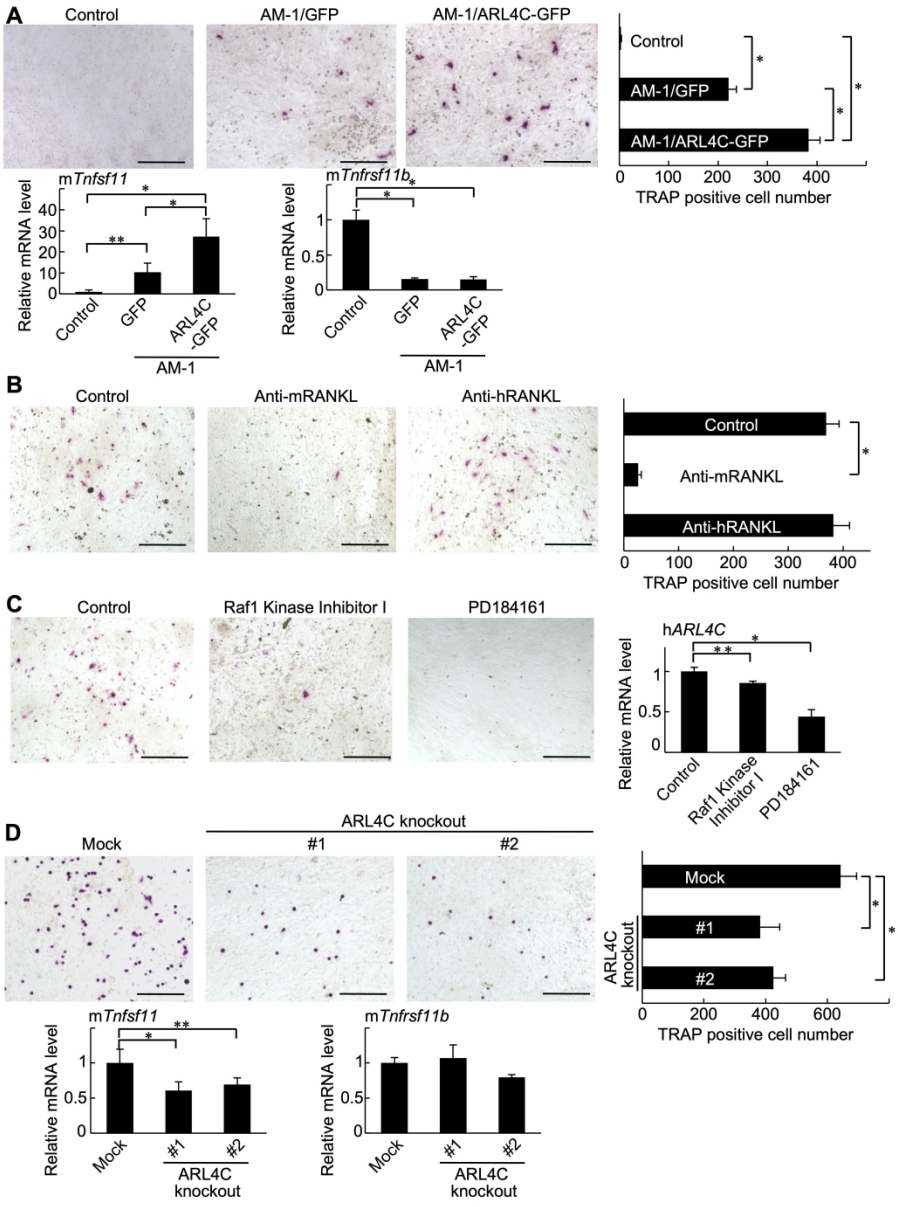

Figure 6: ARL4C expression in ameloblastoma induces osteoclast formation indirectly.

Supporting Information

ARL4C expression, due to RAF1-MEK/ERK pathway, promotes ameloblastoma cell proliferation and osteoclast formation

A short running title: ARL4C expression in ameloblastoma

Shinsuke Fujii[1*], Takuma Ishibashi[1 †], Megumi Kokura[1 †], Tatsufumi Fujimoto[1], Shinji Matsumoto[2,3], Satsuki Shidara[1,11], Kari J Kurppa[4], Judith Pape[5], Javier Caton[6], Peter R Morgan[7], Kristiina Heikinheimo[8], Akira Kikuchi[2], Eijiro Jimi[9,10] and Tamotsu Kiyoshima[1]

[1]Laboratory of Oral Pathology, Division of Maxillofacial Diagnostic and Surgical Sciences, Faculty of Dental Science, Kyushu University, 3-1-1 Maidashi, Higashi-ku, Fukuoka 812-8582, Japan

[2]Department of Molecular Biology and Biochemistry, Graduate School of Medicine, Osaka University, 2-2 Yamadaoka, Suita 565-0871, Japan

[3]Integrated Frontier Research for Medical Science Division, Institute for Open and Transdisciplinary Research Initiatives (OTRI), Osaka University, Suita 565-0871, Japan

[4]Institute of Biomedicine and MediCity Research Laboratories, University of Turku, and Turku Bioscience Centre, University of Turku and Åbo Akademi University, Turku, FI-20520, Finland

[5]Division of Surgery and Interventional Science, Department of Targeted Intervention, Centre for 3D Models of Health and Disease, University College London, Gower Street, London, WC1E 6BT, UK

[6]Department of Anatomy and Embryology, Faculty of Medicine, University Complutense Madrid, 28040 Madrid, Spain

[7]Head & Neck Pathology, King's College London, Guy's Hospital, London, SE1 9RT, UK

[8]Department of Oral and Maxillofacial Surgery, Institute of Dentistry, University of Turku and Turku University Hospital, FI-20520, Finland

[9]Oral Health/Brain Health/Total Health Research Center, Faculty of Dental Science, Kyushu University, 3-1-1 Maidashi, Higashi-ku, Fukuoka 812-8582, Japan

[10]Laboratory of Molecular and Cellular Biochemistry, Faculty of Dental Science, Kyushu University, 3-1-1 Maidashi, Higashi-ku, Fukuoka 812-8582, Japan

[11]Present address: Department of Orthodontics, Tokyo Dental College, 1-2-2 Masago, Mihamaku, Chiba 261-8502, Japan

[†]These authors contributed equally to this work as second authors.

[*]Corresponding author. Laboratory of Oral Pathology, Division of Maxillofacial Diagnostic and Surgical Sciences, Faculty of Dental Science, Kyushu University
3-1-1 Maidashi, Higashi-ku, Fukuoka 812-8582, Japan
Phone: +81-92-642-6328; Fax: +81-92-642-6329
E-mail: sfujii@dent.kyushu-u.ac.jp

Supplementary Materials and methods

Immunohistochemistry

Immunohistochemical staining was performed on 5-μm-thick paraffin sections. Antigen retrieval (Dako, Carpentaria, CA, USA), elimination of the endogenous peroxidase activity (Dako), and blocking (Dako) were carried out as previously mentioned [23,24]. Then the sections were reacted with each primary antibody (used at 1:100 for ARL4C, RAF1 or BRAF V600E) at 4°C overnight. The sections were incubated with secondary antibody (Histofine Simple Stain MAX PO, Nichirei, Tokyo, Japan) for 1 h at RT. The immunoreactivity was visualized with DAB substrate solution (Histofine). Subsequently, the sections were counterstained with hematoxylin. When the total area of a tumor lesion showed >40% staining, the results were defined as ARL4C, RAF1 or BRAF V600E positive. ARL4C (ab122025), RAF1 (ab137435) or BRAF V600E (ab228461) antibody was obtained from Abcam (Cambridge, UK).

Cell lines and reagents

When necessary, the inhibitors, PD184161 (Sigma-Aldrich, Steinheim, Germany), Raf1 Kinase Inhibitor I (Merck Millipore, Darmstadt, Germany), SB590885 (Sigma-Aldrich), PD168393 (Merck Millipore) or SecinH3 (TOCRIS Bioscience, Bristol, UK) were used. Dabrafenib (GSK2118436), Vemurafenib, and anti-phospho-ERK1/2 (Thr202/Tyr204) (4370), anti-ERK1/2 (4695S) and anti-Arf6 (3546) antibodies were obtained from Cell Signaling Technology (Beverly, MA, USA). Anti-β-catenin (610153) and anti-β-actin (A5441) antibodies were from BD Biosciences (San Jose, CA, USA) and Sigma-Aldrich, respectively. BRAF (ab33899) antibody was obtained from Abcam. Anti-Cathepsin K (sc-48353) antibody was obtained from Santa Cruz Biotechnology (Dallas, TX, USA).

Rat anti-mouse RANKL neutralizing monoclonal antibody and mouse anti-human RANKL monoclonal antibody were obtained from Oriental Yeast Co., Tokyo, Japan.

Plasmid construction and infection using lentivirus harboring a cDNA

To generate AM-1 cells that stably express GFP, ARL4C-GFP or ARF6^{Q67L}, parental cells (5×10^4 cells/well in a 12-well plate) were treated with lentivirus and 10 μg/mL polybrene. The cells were then centrifuged at 1200 × *g* for 1 h, and incubated for another 24 h. The incubated cells demonstrating stable expression of GFP or ARL4C-GFP were selected and maintained in culture medium containing 5 μg/mL Blasticidin S (FUJIFILM Wako, Osaka, Japan) [27].

References

23. Matsumoto S, Kurimoto T, Taketo MM*, et al.* The WNT/MYB pathway suppresses KIT expression to control the timing of salivary proacinar differentiation and duct formation. *Development* 2016; **143**: 2311-2324.
24. Mikami Y, Fujii S, Kohashi KI*, et al.* Low-grade myofibroblastic sarcoma arising in the tip of the tongue with intravascular invasion: A case report. *Oncol Lett* 2018; **16**: 3889-3894.
27. Hasegawa K, Fujii S, Matsumoto S*, et al.* YAP signaling induces PIEZO1 to promote oral squamous cell carcinoma cell proliferation. *J Pathol* 2021; **253**: 80-93.

Supplementary Figure Legends

Figure S1. ARL4C expression depends on RAF1-MEK/ERK pathway in ameloblastoma.

(A) AM-1 cells were transfected with control or β-catenin siRNA. Cell lysates were probed with anti-ARL4C, anti-β-catenin and anti-β-actin antibodies (left panels). AM-1 cells were cultured without or with 10 μM PD168393 for 24 h. Cell lysates were probed with anti-ARL4C, anti-phospho-ERK1/2, anti-ERK1/2 and anti-β-actin antibodies (middle panels). AM-1 cells were transfected with control or β-catenin siRNA, and were cultured without or with 10 μM PD168393 for 24 h. Cell lysates were probed with anti-ARL4C, anti-phospho-ERK1/2, anti-ERK1/2, anti-β-catenin and anti-β-actin antibodies (right panels). (B) AM-1 cells were cultured without or with 1 μM Dabrafenib, 1 μM Vemurafenib or 1 μM Raf1 Kinase Inhibitor I for 24 h. Cell lysates were probed with anti-ARL4C, anti-phospho-ERK1/2, anti-ERK1/2 and anti-β-actin antibodies. (C) AM-1 cells were transfected with control or four independent BRAF or RAF1 siRNAs, and *BRAF* or *RAF1* mRNA levels were measured by quantitative RT-PCR. Relative *BRAF* or *RAF1* mRNA levels were normalized by *GAPDH* and expressed as fold-changes compared with levels in control siRNA transfected cells. Cell lysates were probed with anti-BRAF, anti-RAF1 or anti-β-actin antibody. (D) AM-1 cells were cultured without or with 0.1, 0.5, 1 and 10 μM Raf1 Kinase Inhibitor I for 24 h, and then cell lysates were probed with anti-ARL4C, anti-phospho-ERK1/2 or anti-ERK1/2 antibody. (E) AM-1 cells were cultured without or with 10 μM SB590885 and/or 1 μM Raf1 Kinase Inhibitor I for 24 h, and then cell lysates were probed with anti-ARL4C, anti-phospho-ERK1/2, anti-ERK1/2 or anti-β-actin antibody. (F) AM-1 cells were cultured without or with 10 μM PD184161, 10 μM Raf1 Kinase Inhibitor I or 10 μM SB590885 for 24 h, and *EGR1*,

FOSL1, *CCND1* or *C-Myc* mRNA levels were measured by quantitative RT-PCR. Relative *EGR1*, *FOSL1*, *CCND1* or *C-Myc* mRNA levels were normalized by *GAPDH* and expressed as fold-changes compared with levels in control cells. (G) Percentages of RAF1-positive or -negative cases in ameloblastoma or ameloblastoma, unicystic type, or in mandible or maxilla are shown. (H) *RAF1* mRNA levels in HeLaS3, AM-1, AB10 and ABSV cells were measured by quantitative RT-PCR. Relative levels of *ARL4C* mRNA expression were normalized to *GAPDH* and expressed as fold-changes compared with expression in HeLaS3 cells. Results are shown as means ± s.d. of three independent experiments. * $P < 0.01$. **$P < 0.05$.

Figure S2. The effect of BRAF V600E signaling on the proliferation of ameloblastoma cells.

(A) AM-1 cells were cultured without or with 0.1, 1 and 5 μM SB590885 for the indicated numbers of days, and cell numbers were counted. (B) AM-1 cells expressing GFP or ARL4C-GFP were cultured without or with 5 μM SB590885 for the indicated numbers of days, and cell numbers were counted. *$P < 0.01$.

Figure S3. ARL4C expression is involved in the migration of ameloblastoma cells.

(A) AM-1 cells were transfected with control or two independent ARL4C siRNAs, and *ARL4C* mRNA levels were measured by quantitative RT-PCR. Relative *ARL4C* mRNA levels were normalized by *GAPDH* and expressed as fold-changes compared with levels in control siRNA transfected cells. Cell lysates were probed with anti-ARL4C and anti-β-actin antibodies. (B) AM-1 cells were transfected with control or two different ARL4C siRNAs, and then the cells were placed in Transwell chamber for the migration assay.

Migration activities are expressed as the percentage of control cells. (C, D) AM-1 cells expressing GFP or ARL4C-GFP were transfected with control or ARL4C #1 siRNA. (C) Cell lysates were probed with anti-ARL4C and anti-β-actin antibodies. (D) The cells were placed in Transwell chamber for the migration assay. Migration activities are expressed as the percentage of control cells. Scale bars, 200 μm. *$P < 0.01$. **$P < 0.05$.

Figure S4. Generation of ARL4C knockout cells.

(A) Schematic drawing of the targeting site of the single guide RNA at exon of human ARL4C gene. (B) Sequences of ARL4C with PAM sequences labeled in red in knockout AM-1 cells are shown. Blue letter indicates mutated nucleotide. (C) ARL4C control or knockout AM-1 cells were placed in Transwell chamber for the migration assay. Migration activities are expressed as the percentage of control cells. Scale bars, 200 μm. *$P < 0.01$.

Figure S5. ARL4C expression in ameloblastoma tissues.

Ameloblastoma tissues, which were located in bone tissue, were stained with H&E. Dashed box and solid box indicate enlarged images. White arrowheads indicate osteoclasts. Representative ameloblastoma tissue stained with anti-ARL4C antibody, and hematoxylin was shown (dashed box). Dotted lines and black lines indicate the border between ameloblastoma and stroma, and between bone and stroma, respectively. Scale bar, 100 μm.

Figure S6. ARL4C expression in ameloblastoma induces osteoclast formation.

(A, B) AM-1 cells expressing ARL4C-GFP (2×10^4 cells) and mouse BMCs (2×10^6

cells) were co-cultured with POBs (1×10^4 cells) for 7 days in 48-well plates. (A) After 7 days of culture, cells were fixed and stained for TRAP. Box shows enlarged image. (B) The bone-resorbing activity of osteoclasts was assessed using an Osteo Assay Plate after 7 days of culture. Cells were removed by the 5% of hypochlorous acid solution. Resorption pits (black arrowheads) were observed under a microscopy. (C) Human *TNFSF11* or human *TNFRSF1B* mRNA levels in HeLaS3, A549, SAS, NCI-H520 and AM-1 cells were measured by quantitative RT-PCR. Relative levels of human *TNFSF11* or human *TNFRSF1B* levels were normalized to *GAPDH* and expressed as fold-changes compared with expression in HeLaS3 cells. (D) Human *TNFSF11* or human *TNFRSF1B* mRNA levels were measured by quantitative RT-PCR. Relative human *TNFSF11* or human *TNFRSF1B* mRNA levels were normalized by human *GAPDH* and expressed as fold-changes compared with levels in control cells. (E) AM-1 cells and mouse BMCs were co-cultured with POBs without or with 10 μM PD184161 or 10 μM Raf1 Kinase Inhibitor I for initial 2 days and cultured for total 7 days in 48-well plates. After the culture, cells were fixed and stained for TRAP and TRAP-positive cells were counted. (F) A schematic model of RAF1-MEK/ERK-dependent ARL4C expression and its function in ameloblastoma. Results are shown as means ± s.d. of three independent experiments. **P* < 0.01. Scale bars, 100 μm (A), 200μm (B).

Table S1. The clinicopathological data of the patients with ameloblastoma.

Sample no.	Age	Sex	Location	Histology	Size (Mesiodistal× buccolingual× vertical)	Primary/ recurrence	IHC		
							ARL4C	BRAF V600E	RAF1
1	16	Male	Left posterior mandible	Ameloblastoma, unicystic type (luminal type)	23.2×17.8×36.0	1st recurrence	−	+	+
2	40	Female	Left posterior mandible	Ameloblastoma (follicular type)	30.0×16.0×20.0	Primary	+	+	+
3	42	Male	Left mandible	Ameloblastoma (follicular type)	25.0×15.0×44.0	Primary	+	+	+
4	32	Male	Right posterior mandible	Ameloblastoma, unicystic type (luminal type)	38.4×35.3×60.0	1st recurrence	−	−	−
5	13	Female	Right posterior mandible	Ameloblastoma (plexiform type)	26.4×23.4×19.3	Primary	+	−	+
6	39	Male	Mandible	Ameloblastoma (plexiform type)	80.0×20.7×31.4	Primary	+	−	−
7	40	Male	Left posterior mandible	Ameloblastoma (follicular type)	35.0×23.0×13.4	1st recurrence	+	+	+
8	54	Male	Right posterior maxilla	Ameloblastoma (plexiform type)	30.0×14.1×9.7	Primary	+	+	+
9	30	Female	Right body mandible	Ameloblastoma (plexiform type)	42.3×25.0×21.3	Primary	+	+	+
10	51	Male	Middle anterior mandible	Ameloblastoma (follicular type)	54.0×14.0×53.0	1st recurrence	+	−	+
11	12	Female	Right posterior mandible	Ameloblastoma (plexiform type)	64.5×28.7×34.0	1st recurrence	−	+	+
12	60	Male	Left posterior mandible	Ameloblastoma (follicular type)	52.7×19.1×47.0	Primary	+	−	−
13	19	Female	Left posterior mandible	Ameloblastoma, unicystic type (luminal type)	31.7×20.9×61.9	Primary	+	+	+
14	39	Male	Right mandible	Ameloblastoma, unicystic type (luminal type)	43.9×28.3×35.7	Primary	−	+	+
15	16	Male	Left posterior mandible	Ameloblastoma, unicystic type (luminal type)	72.8×54.1×29.1	Primary	+	−	+
16	20	Female	Left posterior mandible	Ameloblastoma, unicystic type (luminal type)	31.7×20.9×61.9	Primary	−	+	+
17	45	Male	Left mandible	Ameloblastoma (plexiform type)	16.8×10.3×19.5	Primary	−	−	+
18	44	Male	Middle anterior mandible	Ameloblastoma (follicular type)	14.5×14.1×20.9	Primary	+	−	+

19	18	Male	Left posterior mandible	Ameloblastoma (plexiform type)	27.6×20.8×20.2	Primary	+	+	+
20	33	Female	Right mandible	Ameloblastoma, unicystic type (luminal type)	43.3×24.0×24.2	Primary	−	−	+
21	66	Male	Left posterior mandible	Ameloblastoma (plexiform type)	33.9×14.1×13.8	Primary	+	+	+
22	18	Male	Right mandible	Ameloblastoma (plexiform type)	51.6×36.4×28.6	Primary	+	+	+
23	14	Female	Middle anterior mandible	Ameloblastoma (plexiform type)	59.2×31.5×28.7	Primary	+	+	+
24	32	Female	Right posterior mandible	Ameloblastoma (follicular type)	27.5×16.7×22.3	Primary	+	+	+
25	49	Male	Mandible	Ameloblastoma (plexiform type)	2.8×26.4×24.0	Primary	+	+	+
26	60	Male	Right body mandible	Ameloblastoma (follicular type)	70.9×17.7×28.0	3rd recurrence	+	+	+
27	15	Male	Right posterior mandible	Ameloblastoma (plexiform type)	75.6×28.2×120.0	Primary	−	+	−
28	48	Female	Left maxilla	Ameloblastoma (plexiform type)	61.4×35.9×37.2	Primary	+	+	+
29	64	Male	Left maxilla	Ameloblastoma (plexiform type)	35.2×25.4×50.0	1st recurrence	−	−	−
30	66	Male	Left maxilla	Ameloblastoma (plexiform type)	31.3×24.7×42.0	1st recurrence	+	−	−
31	54	Male	Left body maxilla	Ameloblastoma (plexiform type)	30.0×14.1×9.7	Primary	+	−	−
32	61	Male	Left maxilla	Ameloblastoma (plexiform type)	31.2×16.4×26.3	Primary	+	−	+
33	36	Male	Left mandible	Ameloblastoma (plexiform type)	33.6×29.1×29.2	Primary	+	+	+
34	28	Female	Right mandible	Ameloblastoma (plexiform type)	26.5×16.7×13.3	Primary	+	+	+
35	56	Female	Middle anterior mandible	Ameloblastoma (follicular type)	13.2×10.2×11.0	Primary	+	+	+
36	39	Female	Left anterior maxilla	Ameloblastoma (plexiform type)	29.2×18.8×17.7	Primary	+	+	+
37	73	Female	Mandible	Ameloblastoma (plexiform type)	51.5×35.2×75.6	Primary	−	+	+
38	23	Male	Right posterior mandible	Ameloblastoma (plexiform type)	30.8×23.4×41.3	Primary	+	+	+

Size was calculated by computed tomography scan.

Radiographically, image characteristics of ameloblasotma and ameloblastoma, unicystic type were multilocular and unilocular, respectively.

Table S2. Designs for siRNAs used in this study.

siRNA	Sequence
Human RAF1 #1	GCAAAGAACAGTGGTCAAT
Human RAF1 #2	GGATTTCGATGTCAGACTT
Human RAF1 #3	GCTGCATCTCTCCTACAAT
Human RAF1 #4	GCTTGCATGACTGCCTTAT
Human BRAF #1	CCAACTTGATTTGCTGTTT
Human BRAF #2	GCATCAATGGATACCGTTA
Human BRAF #3	GCTGTGCTGTTTACAGAAT
Human BRAF #4	GGAAGTGTTGGAGAATGTT
Human ARL4C #1	GGCTGTGAAGCTGAGTAAT
Human ARL4C #2	GAGTGCGTCAAGAAAGAAT
Human β-catenin	CCCACTAATGTCCAGCGTT
randomized control	CAGTCGCGTTTGCGACTGG

Table S3. Quantitative RT-PCR primers used in this study.

Gene	Primers
human ARL4C	Forward 5′-CTAACATCTCGGCCTTCCAG-3′ Reverse 5′-TCTGCTTGAGGGACTTCCTG-3′
human BRAF	Forward 5′-ACCACCCAATACCACAGGAA-3′ Reverse 5′-CATTGGGAGCTGATGAGGAT-3′
human RAF1	Forward 5′-ACCCATTCAGTTTCCAGTCG-3′ Reverse 5′-GCTACCAGCCTCTTCATTGC-3′
human EGR1	Forward 5′-TGACCGCAGAGTCTTTTCCT-3′ Reverse 5′-TGGGTTGGTCATGCTCACTA-3′
human FOSL1	Forward 5′-AGCTGCAGAAGCAGAAGGAG-3′ Reverse 5′-GGAGTTAGGGAGGGTGTGGT-3′
human CCND1	Forward 5′-GATGCCAACCTCCTCAACGA-3′ Reverse 5′-GGAAGCGGTCCAGGTAGTTC-3′
human C-Myc	Forward 5′-TTCGGGTAGTGGAAAACCAG-3′ Reverse 5′-CAGCAGCTCGAATTTCTTCC-3′
human RANKL	Forward 5′-AGAGCGCAGATGGATCCTAA-3′ Reverse 5′-TTCCTTTTGCACAGCTCCTT-3′
human OPG	Forward 5′-GGCAACACAGCTCACAAGAA-3′ Reverse 5′-CTGGGTTTGCATGCCTTTAT-3′
human GAPDH	Forward 5′-GCACCGTCAAGGCTGAGAAC-3′ Reverse 5′-TGGTGAAGACGCCAGTGGA-3′
mouse RANKL	Forward 5′-AGCCGAGACTACGGCAAGTA-3′ Reverse 5′-GCGCTCGAAAGTACAGGAAC-3′
mouse OPG	Forward 5′-CTGCCTGGGAAGAAGATCAG-3′ Reverse 5′-TTGTGAAGCTGTGCAGGAAC-3′
mouse GAPDH	Forward 5′-TGTGTCCGTCGTGGATCTGA-3′ Reverse 5′-TTGTGAAGCTGTGCAGGAAC-3′

Fujii et al., Figure S1

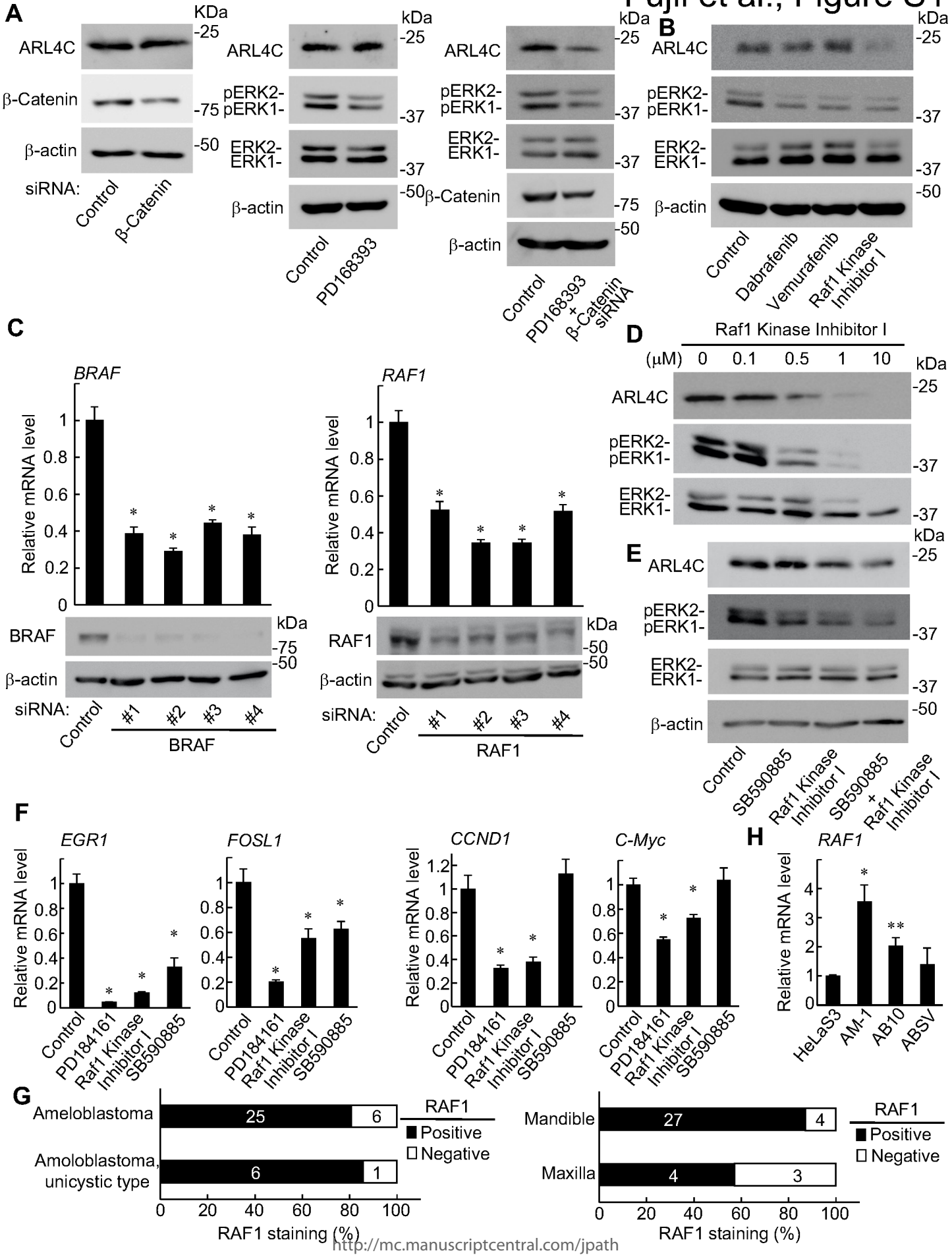

Figure S1. ARL4C expression depends on RAF1-MEK/ERK pathway in ameloblastoma.
(A) AM-1 cells were transfected with control or β-catenin siRNA. Cell lysates were probed with anti-ARL4C, anti-β-catenin and anti-β-actin antibodies (left panels). AM-1 cells were cultured without or with 10 μM PD168393 for 24 h. Cell lysates were probed with anti-ARL4C, anti-phospho-ERK1/2, anti-ERK1/2 and anti-β-actin antibodies (middle panels). AM-1 cells were transfected with control or β-catenin siRNA, and were cultured without or with 10 μM PD168393 for 24 h. Cell lysates were probed with anti-ARL4C, anti-phospho-ERK1/2, anti-ERK1/2, anti-β-catenin and anti-β-actin antibodies (right panels). (B) AM-1 cells were cultured without or with 1 μM Dabrafenib, 1 μM Vemurafenib or 1 μM Raf1 Kinase Inhibitor I for 24 h. Cell lysates were probed with anti-ARL4C, anti-phospho-ERK1/2, anti-ERK1/2 and anti-β-actin antibodies. (C) AM-1 cells were transfected with control or four independent BRAF or RAF1 siRNAs, and *RAF1* or *BRAF* mRNA levels were measured by quantitative RT-PCR. Relative *BRAF* or *RAF1* mRNA levels were normalized by *GAPDH* and expressed as fold-changes compared with levels in control siRNA transfected cells. Cell lysates were probed with anti-BRAF, anti-RAF1 or anti-β-actin antibody. (D) AM-1 cells were cultured without or with 0.1, 0.5, 1 and 10 μM Raf1 Kinase Inhibitor I for 24 h, and then cell lysates were probed with anti-ARL4C, anti-phospho-ERK1/2 or anti-ERK1/2 antibody. (E) AM-1 cells were cultured without or with 10 μM SB590885 and/or 1 μM Raf1 Kinase Inhibitor I for 24 h, and then cell lysates were probed with anti-ARL4C, anti-phospho-ERK1/2, anti-ERK1/2 or anti-β-actin antibody. (F) AM-1 cells were cultured without or with 10 μM PD184161, 10 μM Raf1 Kinase Inhibitor I or 10 μM SB590885 for 24 h, and *EGR1*, *FOSL1*, *CCND1* or *C-Myc* mRNA levels were measured by quantitative RT-PCR. Relative *EGR1*, *FOSL1*, *CCND1* or *C-Myc* mRNA levels were normalized by *GAPDH* and expressed as fold-changes compared with levels in control cells. (G) Percentages of RAF1-positive or -negative cases in amaloblastoma or amaloblastoma, unicystic type, or in mandible or maxilla are shown. (H) *RAF1* mRNA levels in HeLaS3, AM-1, AB10 and ABSV cells were measured by quantitative RT-PCR. Relative levels of *ARL4C* mRNA expression were normalized to *GAPDH* and expressed as fold-changes compared with expression in HeLaS3 cells. Results are shown as means ± s.d. of three independent experiments. * $P < 0.01$. ** $P < 0.05$.

Fujii et al., Figure S2

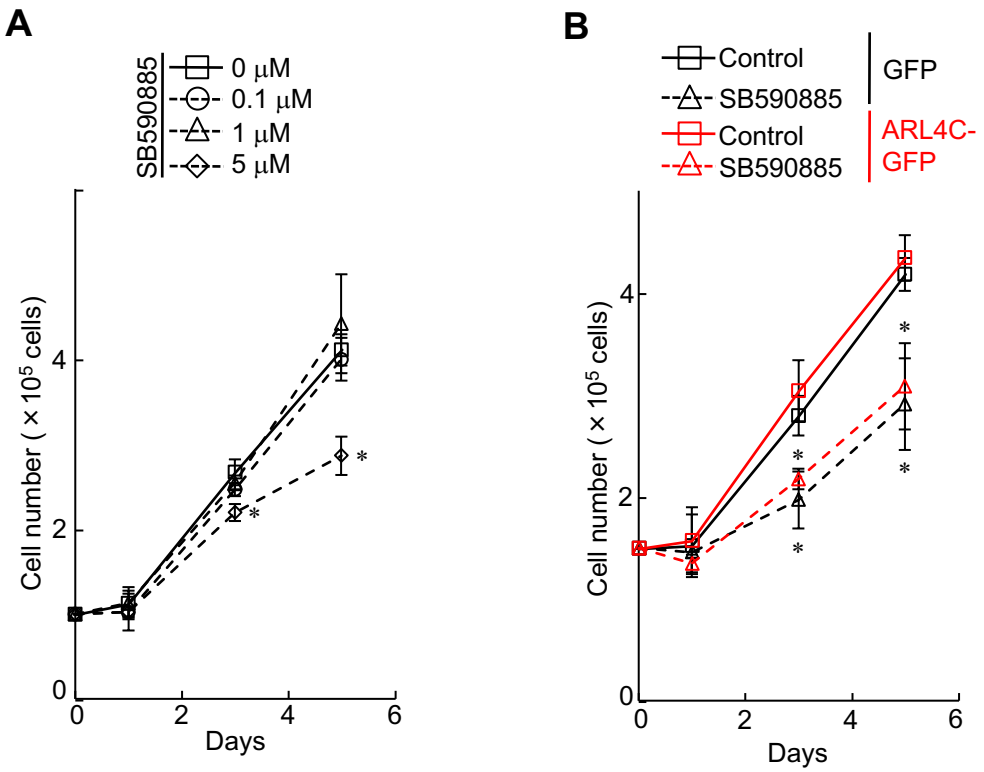

Figure S2. The effect of BRAF V600E signaling on the proliferation of ameloblastoma cells. (A) AM-1 cells were cultured without or with 0.1, 1 and 5 μM SB590885 for the indicated numbers of days, and cell numbers were counted. (B) AM-1 cells expressing GFP or ARL4C-GFP were cultured without or with 5 μM SB590885 for the indicated numbers of days, and cell numbers were counted. *$P < 0.01$.

Fujii et al., Figure S3

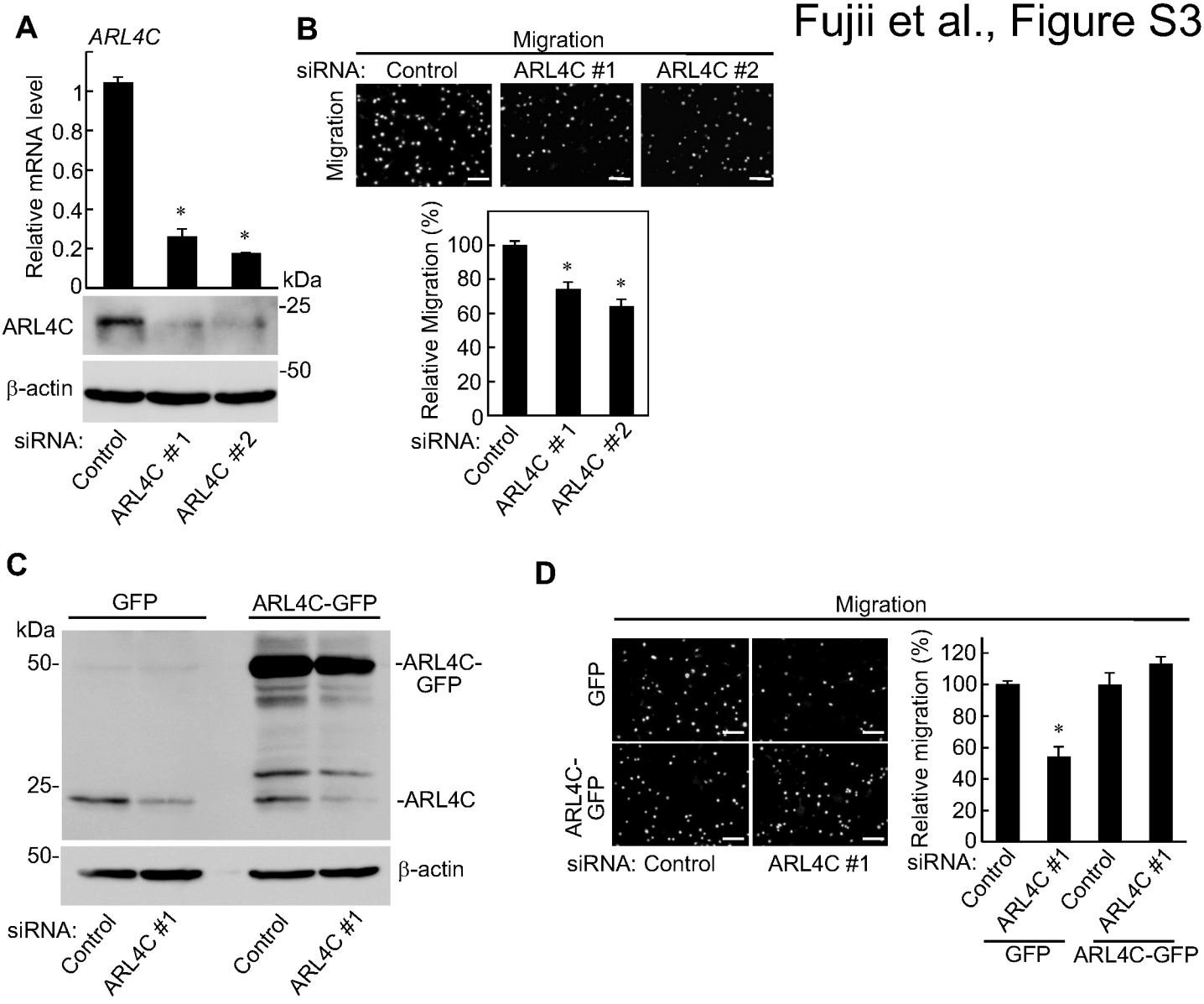

Figure S3. ARL4C expression is involved in the migration of ameloblastoma cells.
(A) AM-1 cells were transfected with control or two independent ARL4C siRNAs, and *ARL4C* mRNA levels were measured by quantitative RT-PCR. Relative *ARL4C* mRNA levels were normalized by *GAPDH* and expressed as fold-changes compared with levels in control siRNA transfected cells. Cell lysates were probed with anti-ARL4C and anti-β-actin antibodies. (B) AM-1 cells were transfected with control or two different ARL4C siRNAs, and then the cells were placed in Transwell chamber for the migration assay. Migration activities are expressed as the percentage of control cells. (C, D) AM-1 cells expressing GFP or ARL4C-GFP were transfected with control or ARL4C #1 siRNA. (C) Cell lysates were probed with anti-ARL4C and anti-β-actin antibodies. (D) The cells were placed in Transwell chamber for the migration assay. Migration activities are expressed as the percentage of control cells. Scale bars, 200 μm. *$P < 0.01$.

Fujii et al., Figure S4

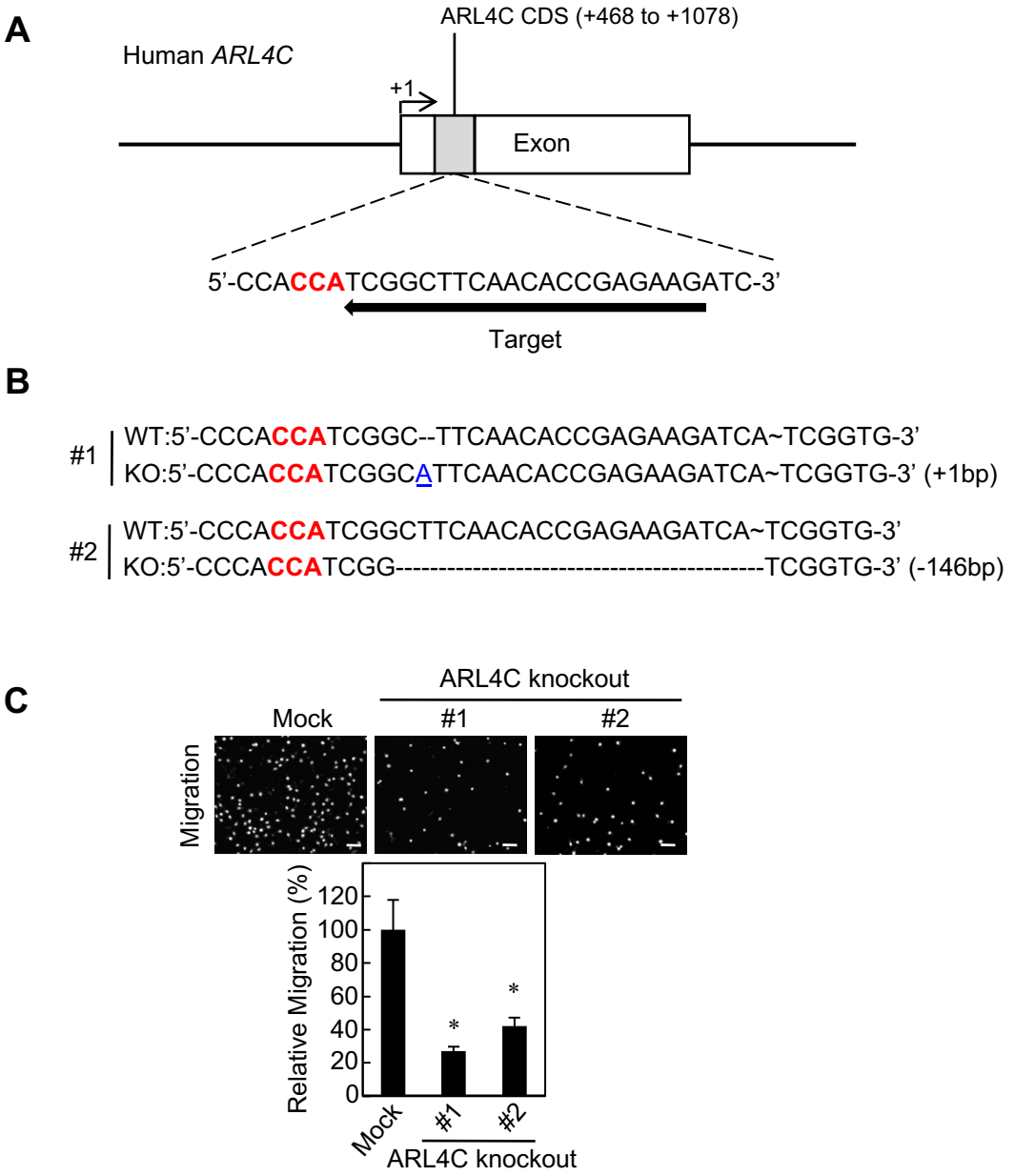

Figure S4. Generation of ARL4C knockout cells.
(A) Schematic drawing of the targeting site of the single guide RNA at exon of human ARL4C gene. (B) Sequences of ARL4C with PAM sequences labeled in red in knockout AM-1 cells are shown. Blue letter indicates mutated nucleotide. (C) ARL4C control or knockout AM-1 cells were placed in Transwell chamber for the migration assay. Migration activities are expressed as the percentage of control cells. Scale bars, 200 μm. *$P < 0.01$.

Fujii et al., Figure S5

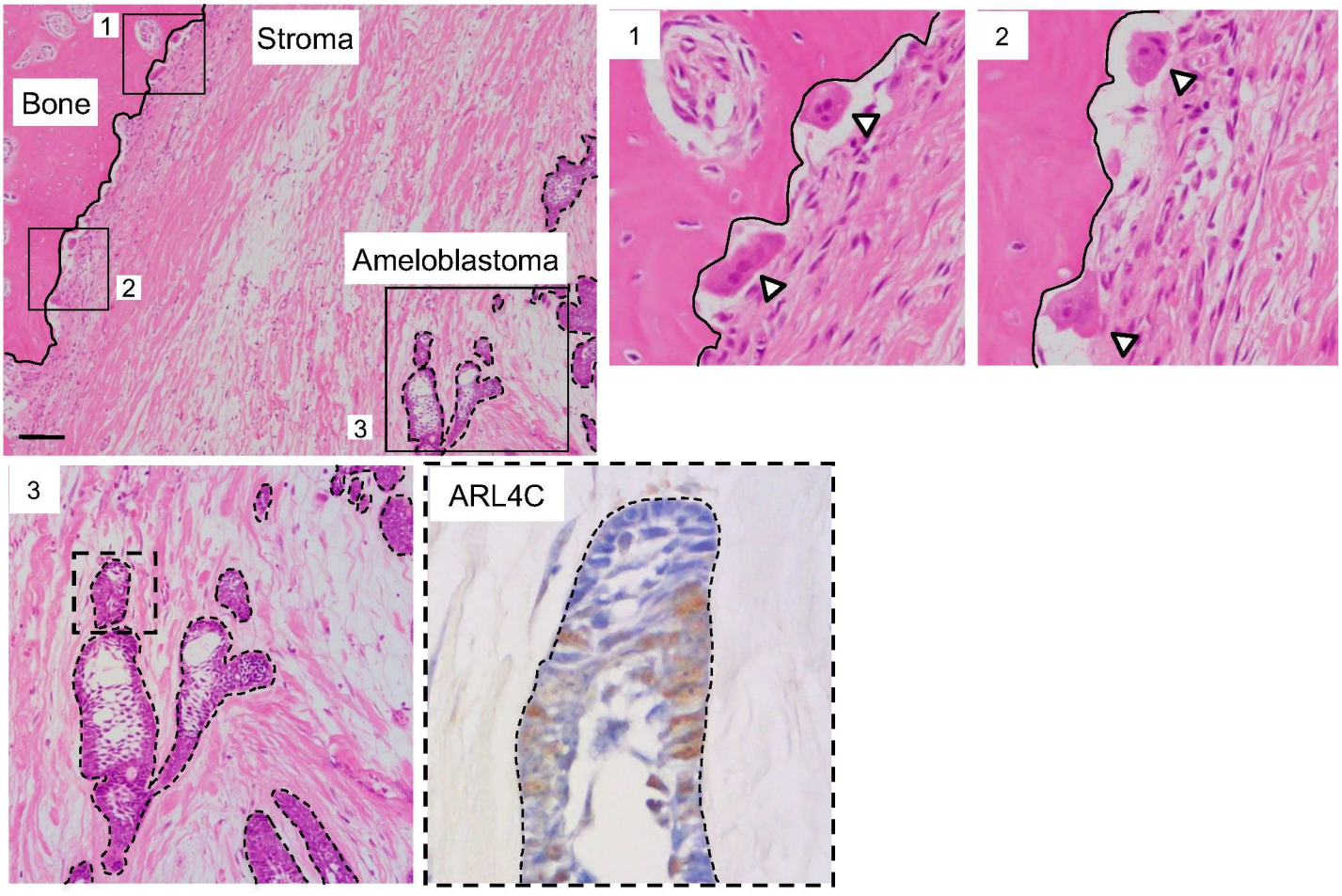

Figure S5. ARL4C expression in ameloblastoma tissues.
Ameloblastoma tissues, which were located in bone tissue, were stained with H&E. Dashed box and solid box indicate enlarged images. White arrowheads indicate osteoclasts. Representative ameloblastoma tissue stained with anti-ARL4C antibody, and hematoxylin was shown (dashed box). Dotted lines and black lines indicate the border between ameloblastoma and stroma, and between bone and stroma, respectively. Scale bar, 100 μm.

Fujii et al., Figure S6

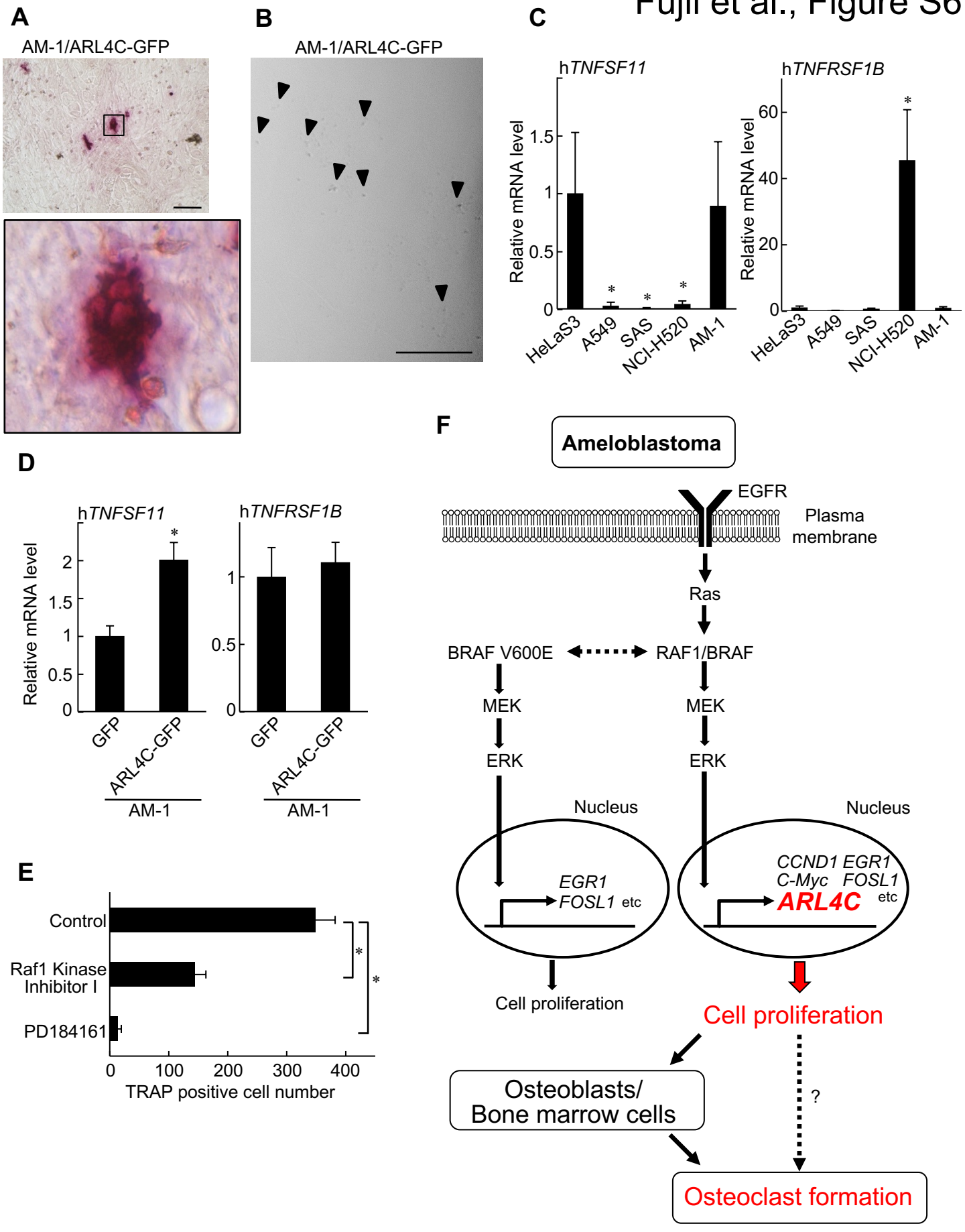

Figure S6. ARL4C expression in ameloblastoma induces osteoclast formation.
(A, B) AM-1 cells expressing ARL4C-GFP (2×10^4 cells) and mouse BMCs (2×10^6 cells) were co-cultured with POBs (1×10^4 cells) for 7 days in 48-well plates. (A) After 7 days of culture, cells were fixed and stained for TRAP. Box shows enlarged image. (B) The bone-resorbing activity of osteoclasts was assessed using an Osteo Assay Plate after 7 days of culture. Cells were removed by the 5% of hypochlorous acid solution. Resorption pits (black arrowheads) were observed under a microscopy. (C) Human *TNFSF11* or human *TNFRSF1B* mRNA levels in HeLaS3, A549, SAS, NCI-H520 and AM-1 cells were measured by quantitative RT-PCR. Relative levels of human *TNFSF11* or human *TNFRSF1B* levels were normalized to *GAPDH* and expressed as fold-changes compared with expression in HeLaS3 cells. (D) Human *TNFSF11* or human *TNFRSF1B* mRNA levels were measured by quantitative RT-PCR. Relative human *TNFSF11* or human *TNFRSF1B* mRNA levels were normalized by human *GAPDH* and expressed as fold-changes compared with levels in control cells. (E) AM-1 cells and mouse BMCs were co-cultured with POBs without or with 10 μM PD184161 or 10 μM Raf1 Kinase Inhibitor I for initial 2 days and cultured for total 7 days in 48-well plates. After the culture, cells were fixed and stained for TRAP and TRAP-positive cells were counted. (F) A schematic model of RAF1-MEK/ERK-dependent ARL4C expression and its function in ameloblastoma. Results are shown as means ± s.d. of three independent experiments. $^*P < 0.01$. Scale bars, 100 μm (A), 200μm (B).